TABLE 3. Surgery and Postoperative Complication in Thirty-One Resected Patients

Variable	Data
Operative procedures	
Pancreaticoduodenectomy	21 (68%)
Caudal pancreatectomy	6 (19%)
Total pancreatectomy	4 (13%)
Vascular resection/reconstruction	
PV/SMV→ end-to-end anastomosis	12 (39%)
Right posterior hepatic artery*	3 (9%)
Common hepatic artery→ end-to-end anastomosis	1 (3%)
IVC→ patched by vein graft	1 (3%)
Postoperative LPC	31 (100%)
Major complication	
Intra-abdominal bleeding	4 (13%)
Intra-abdominal infection	1 (3%)
Liver abscess	1 (3%)
Major bile leakage	1 (3%)
Overall in-hospital mortality rate	0 (0%)

*The right posterior hepatic artery branched from the superior mesenteric artery was involved by cancer and it was resected. Without vascular reconstruction, the hepatic blood-flow was maintained well, due to well-developed vascular network in the liver.
LPC (5FU was infused via both the hepatic artery and portal vein).

their dissected margins were confirmed as cancer-free by the intraoperative cytology in 7 of the 19 patients. The remaining 12 of the 19 patients (63%) were received en bloc resection of the PV/SMV because their PV/SMVs were not isolated from the pancreatic tumors. Three patients had cancer invasion to the right posterior hepatic artery branched from the SMA, and which was resected together with the pancreatic head. Because the hepatic blood flow did not thereby decrease, no vascular reconstruction was added. One patient underwent resection of the common hepatic artery which was partly involved by cancer. An end-to-end anastomosis was safely done between the common hepatic artery and the proper hepatic artery. One patient received a wedge resection of the inferior vena cava which was partly involved by cancer, and its defect was patched up with a saphenous vein graft. The adrenal grand or transverse colon was resected in each one patient because of cancer invasion. Immediately after surgery, all (100%) of the 31 pancreatectomized patients underwent LPC without interruption, and none of them developed grades 2 to 4 toxicity. Consequently, 31 (82%) of 38 registered patients completed the initially scheduled protocol. Postoperative complications developed in 4 of 31 pancreatectomized patients (13%): intra-abdominal bleeding = 1; infection at the site of pancreatic anastomosis = 1; liver abscess = 1; and leakage at the site of choledocojejunostomy = 1. However, all of these were successfully treated without any in-hospital deaths.

Postoperative Outcomes and Patterns of Cancer Recurrence

All 38 patients received preoperative chemoradiation with or without subsequent surgery and the median follow-up period was 39 months (range: 14–72 months). The median survival period was 32 months and the 5-year survival rate was 41% (Fig. 4). For the 7 patients who could not undergo surgical resection, the median survival period was 13 months and the 2-year survival rate was 14% (Fig. 5). In contrast, for the 31 patients who received surgical resection followed by postoperative LPC, the 5-year survival rate was 53%. Likewise, after pancreatectomy, their 2- and 5-year disease-free survival rates were 72% and 59%, respectively. Among

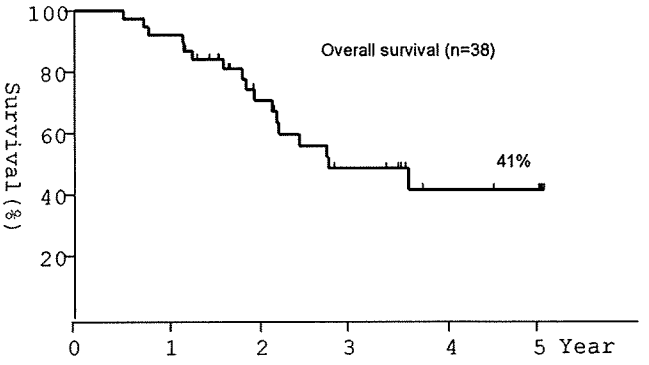

FIGURE 4. Survival curve for 38 patients who received preoperative chemoradiation. The 5-year overall survival rate was 41% in 38 patients who received preoperative chemoradiation.

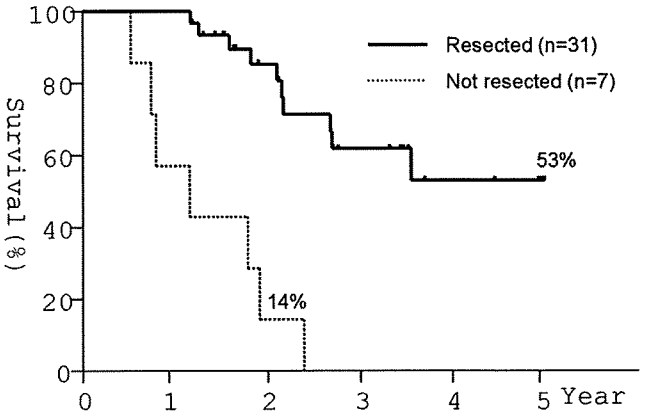

FIGURE 5. Survival curves for 31 resected and 7 unresected cases. The 5-year survival rate was 53% in the 31 patients who received surgical resection followed by LPC. The 2-year survival rate was 14% for the remaining 7 patients who were excluded from surgical resection.

11 patients who developed cancer recurrence, 2 patients (18%) had locoregional disease. Ten patients (91%) had distant metastasis: lung metastasis = 4; peritoneal seeding = 3; liver metastasis = 2, and bone metastasis = 1 (Table 4). At 5 years after operation, the cumulative rate of liver metastasis was 7%, and cumulative rate of local recurrence was 9% (Fig. 6). Among 31 resected patients, there was no significant correlation between the patient survival and CA19 to 9 levels after preoperative treatments.

Microscopic Examination of the Resected Specimens

Microscopically, the pancreatic cancer tissues were replaced by varying amount of fibrous connective tissues. The residual cancer nests included 13 (42%) well-differentiated adenocarcinomas, 15 (48%) moderately differentiated adenocarcinomas, and 3 (10%) poorly differentiated adenocarcinomas. Although all 31 resected patients had been previously diagnosed by imaging techniques before preoperative chemoradiation as having T3-cancer, postoperative microscopic examination of the resected specimens revealed that 4 (13%) patients had p-T1 tumors, 8 (26%) had p-T2 tumors, and 19 (61%) had p-T3 tumors, respectively (Table 5). According to Evans's histopathological criteria, more than 50% of tumor destruction (grade IIb or more) was seen in 21 patients (68%). The surgical

TABLE 4. Sites of Cancer Recurrence in Eleven Patients With Recurrent Disease

Sites	No. Cases
Recurrence	11 (100%)
Local	1 (9%)
Local + distant (liver)	1 (9%)
Distant alone	
Lung	4 (36%)
Peritoneal	3 (27%)
Liver	1 (9%)
Bone	1 (9%)

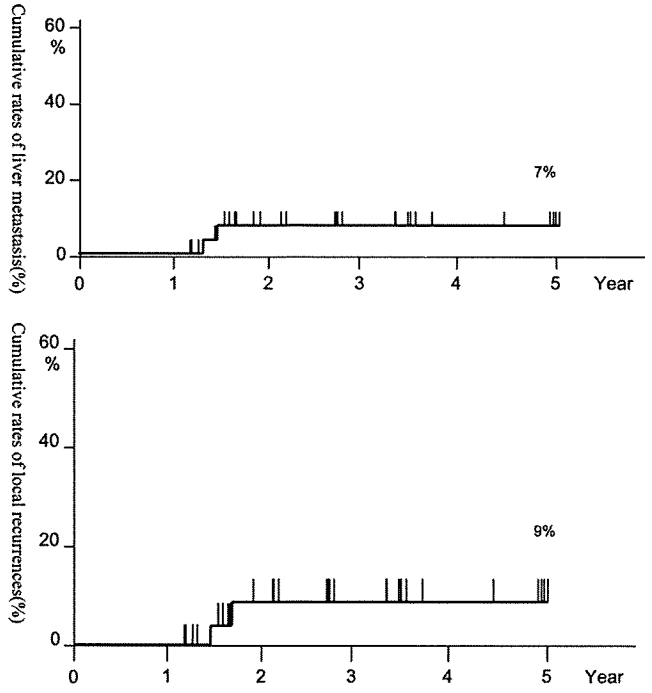

FIGURE 6. Cumulative rates of liver metastasis and local recurrence in 31 resected patients. In the 31 resected patients, the cumulative rate of liver metastasis was 7% at 5-postoperative year (upper figure). The cumulative rate of local recurrence was 9% at 5-postoperative year (lower figure).

margin was judged to be negative for malignancy (R0) for 30 patients (97%) and positive (R1) for 1 patient. Nodal involvement was seen in only 3 (10%) of 31 resected patients, and the cancer invasion to the PV/SMV was detected in 3 patients (25%) of 12 patients who had received PV/SMV-resection. When the 31 resected patients were classified into 2 subgroups, one consisting of 21 patients (pathologic responders) with >50% tumor destruction and one consisting of 10 patients (nonresponder) with <50% tumor destruction, the 5-year survival rate (58% vs. 48%; $P = 0.78$) or 5-year cumulative rate of local recurrence (8% vs. 10%; $P = 0.33$) did not differ significantly between the 2 subgroups. Before chemoradiation, the serum levels of CA19 to 9 were 481 + 884 U/mL in the former subgroup and 217 + 302 U/mL in the latter subgroup, respectively (ns). Likewise, the CA19 to 9 levels after chemoradiation (before operation) did not differ between the 2 subgroups (25 + 20 U/mL vs. 21 + 15 U/mL; ns).

TABLE 5. Microscopic Findings in Thirty-One Resected Cases

Factor	Data
p-T classification	
T0	0 (0%)
T1	4 (13%)
T2	8 (26%)
T3	19 (61%)
Tumor destruction >50%*	21 (68%)
Resection margin	
Negative (R0)	30 (97%)
Positive (R1)	1 (3%)
Nodal involvement	
Negative	28 (90%)
Positive	3 (10%)
PV/SMV invasion	3†

*Grade IIb or more according to Evans's criteria.[20]

†Twenty-five percent among 12 patients who had received PV/SMV resection; or 16% among 19 patients whose PV/SMVs had been diagnosed preoperatively by radiologic imaging as positive for cancer invasion.

DISCUSSION

In our previous study,[23] postoperative cytology was performed for the drained fluid from the pancreatic bed after the R0-resection of locally advanced pancreatic cancer. The result showed that 85% of cytology-positive patients developed locoregional recurrence within 2 postoperative years, suggesting an extreme difficulty in surgically eradicating microscopic residual cancer cells. Spitz et al[24] indicated that postoperative adjuvant therapy was impossible for roughly one quarter of patients due to a high incidence of postoperative complications after pancreatectomy. In addition, Willett et al[25] described no prognostic benefit of postoperative chemoradiation for patients who received R1 or R2-resection. Thus, preoperative downstaging is a very attractive strategy for pancreatic surgeons and there have been an increasing number of reports on chemoradiation before pancreatic cancer resection.

During preoperative irradiation, most authors employed 5-FU infusion, which is not only a systemic cytotoxic agent but also a potent radiosensitizer. Apart from 5-FU, gemcitabine has, in recent years, come to be known as a powerful agent for enhancing the radiosensitivity of human pancreatic cancer cells.[13] Furthermore, there have been an increasing number of reports suggesting that gemcitabine may be preferable to 5-FU for systemic chemotherapy of nonresectable pancreatic cancer.[26] Therefore, we decided to use a combination of gemcitabine infusions and radiation therapy. Some authors[26–28] have shown that the maximum tolerable dose of gemcitabine ranged from 350 to 600 mg/m^2/week when combined with 50 to 55 Gy of conventional external radiation therapy. On the other hand, McGinn et al[14] planned a gross target volume with a 1-cm margin (24–42 Gy) in order not to reduce the dose of gemcitabine (1000 mg/m^2/week). Compared with these regimens, our regimen was somewhat more intensive; a full dose of gemcitabine (1000 mg/m^2/wk) plus 50 Gy of radiation. Nevertheless, all 38 of our patients completed radiation successfully and only 8% required a reduced dose of gemcitabine (600 mg/m^2/wk). As a result, apart from 4 patients who developed distant metastases or local disease progression before the operation, all of the remaining 34 were able to undergo the initially scheduled laparotomy. Such high tolerance rates may be attributable to the scope of our radiation field which did not include any part of the gastrointestinal tracts. The small bowel is one of the most sensitive organs to radiation; especially crypt cells

are very sensitive.[29] In addition, once the mucosal injury is caused by radiation, loss of absorptive function, diarrhea, and cramps with abdominal pain are more likely to develop subsequently. The incidence and severity of bowel injury are related to the dose, target volume, and dose rate of radiation delivery. Therefore, our method of 5 portals radiation used and its planning via 3D-CT may also have played an important role in preventing from the gastrointestinal injury. When the primary pancreatic tumor was close to the stomach or the duodenum, these GI-tracts were excluded from the radiation field but resected concomitantly during the after surgery. Although our radiation field covered a wide range of the retropancreatic spaces, most common site of cancer recurrence, it seemed to have no significant affect on the gastrointestinal toxicity. Future studies utilizing more specific forms of radiation therapy such as intensity-modulated radiotherapy, heavy particle radiotherapy, or proton beam radiation may bring even better results.

Microscopically, the pancreatic cancer tissues treated with preoperative chemoradiation were replaced by various amounts of fibrous connective tissues. Evans et al[20] showed that Grade IIb or more extensive destruction of tumor (>50%) was seen in 7 of 17 patients (41%). Likewise, marked decreases in the incidences of positive margin were reported when preoperative chemoradiation was performed before the surgery: from 56% to 28% by Pendurthi et al[8]; from 26% to 12% by Spitz et al[24]; and from 64% to 30% by White et al.[30] In addition, incidences of nodal involvement were also reported to be thereby decreased: from 87% to 28% by Pendurthi et al[8]; from 63% to 46% by Spitz et al[24]; and from 55% to 31% by White et al.[30] Compared with these figures, more extensive destruction was seen in our 31 patients: the incidence of Grade IIb or higher destruction was 68%; positive surgical margins were a mere 3%; and nodal involvement was 10%. Also, cancer invasion to the PV/SMV was seen in only 3 (25%) patients among 12 patients who had received PV/SMV resections; or 16% among 19 patients whose PV/SMVs had been diagnosed preoperatively by radiologic imaging as positive for cancer invasion.

Thus, the microscopic changes (downstaging) that we witnessed were much more significant than what we had expected based on preoperative CT-images or intraoperative macroscopic inspection. Future study is needed to know whether we are able to omit some operative procedures such as lymphadenectomy, connective tissue clearance,[5] or vascular resection[17] with no fear of cancer remnant, if the patients are treated by preoperative chemoradiation.

The incidence of local recurrence was commonly reported to be 50% or more in patients who had undergone surgery alone and 30% or more in patients who had received surgery plus postoperative chemoradiation.[7] On the other hand, the reported incidence of local recurrence was very low in those who underwent preoperative chemoradiation before surgery: 16% by Pendurthi et al; 12% by Talamonti et al; 10% by Spitz et al; and 9% in the present study. Nonetheless, with median survival periods reported to be a mere 30 months or shorter by many previous authors[8–11] preoperative chemoradiation has not yet reached an acceptable level. For this reason, Breslin et al[9] reported that liver metastasis developed in 41 of 75 patients (55%) who had cancer recurrences after preoperative chemoradiation plus surgery, whereas the incidence of local recurrence decreased to 10%. Other investigators[9,10,24,31–33] also indicated that surgery combined with chemoradiation therapy shifted the mode of cancer recurrence from local recurrence to distant (mainly liver) metastasis. Unfortunately, there have been no previous reports demonstrating a reduction in the incidence of liver metastasis through the use of systemic chemotherapy[34,35] or by prophylactic whole-liver radiation.[36,37] The only positive results seen have been obtained through the use of certain kinds of LPCs via the portal vein[38]; via the hepatic artery[39]; or via a combination of these 2 routes.[15,18,40] These authors speculated that occult micrometastases might have preoperatively lodged in the liver and that they would be killed by a high dose of anticancer drugs infused directly from the liver-supplying vessels. In our LPC studies for instance, the concentration of 5-FU was maintained at a level of under 0.02 μg/mL in the systemic circulation whereas it was over 0.14 μg/mL in the portal venous circulation.[18] Simoyama's in vitro study[41] as well showed that pancreatic cancer cells were killed when they were incubated continuously in 0.1 μg/mL of 5-FU for 3 weeks or longer. As predicted based on these data, all of our patients safely tolerated postoperative LPC without developing catheter-associated troubles, hepatic dysfunction, or serious toxicity (grade 2 or more). Moreover, the incidence of liver metastasis was as low as 6% (2/31), and the 5-year survival rate was elevated to 53%.

Based on these observations, we may conclude that preoperative chemoradiation is a promising strategy for strengthening local control. Likewise, additional treatments enabling us to reduce the incidence of liver metastasis, for instance our LPC, are needed. To improve the long-term outcomes after resection of T3-pancreatic cancers, these 2 types of treatment strategies should be combined together.

ACKNOWLEDGMENTS

The authors thank Dr. Sachiko Tanaka, Dr. Tastuya Ioka, Dr. Tetsuji Ishida, Dr. Reina Takakura, Dr. Yasuna Takano, and Dr. Satoaki Nakamura for their contributions to this manuscript.

REFERENCES

1. Cameron JL, Crist DW, Sitzmann JV, et al. Factors influencing survival after pancreaticoduodenectomy for pancreatic cancer. *Am J Surg.* 1991;161:120–124; discussion 124–125.
2. Conlon KC, Klimstra DS, Brennan MF. Long-term survival after curative resection for pancreatic ductal adenocarcinoma. Clinicopathologic analysis of 5-year survivors. *Ann Surg.* 1996;223:273–279.
3. Willett CG, Lewandrowski K, Warshaw AL, et al. Resection margins in carcinoma of the head of the pancreas. Implications for radiation therapy. *Ann Surg.* 1993;217:144–148.
4. Sobin L, Wittekind C, eds. *TNM Classification of Malignant Tumors.* 6th ed. New York, NY: Wiley-Liss; 2002.
5. Ishikawa O, Ohhigashi H, Sasaki Y, et al. Practical usefulness of lymphatic and connective tissue clearance for the carcinoma of the pancreas head. *Ann Surg.* 1988;208:215–220.
6. Griffin JF, Smalley SR, Jewell W, et al. Patterns of failure after curative resection of pancreatic carcinoma. *Cancer.* 1990;66:56–61.
7. Staley CA, Lee JE, Cleary KR, et al. Preoperative chemoradiation, pancreaticoduodenectomy, and intraoperative radiation therapy for adenocarcinoma of the pancreatic head. *Am J Surg.* 1996;171:118–124; discussion 124–125.
8. Pendurthi TK, Hoffman JP, Ross E, et al. Preoperative versus postoperative chemoradiation for patients with resected pancreatic adenocarcinoma. *Am Surg.* 1998;64:686–692.
9. Breslin TM, Hess KR, Harbison DB, et al. Neoadjuvant chemoradiotherapy for adenocarcinoma of the pancreas: treatment variables and survival duration. *Ann Surg Oncol.* 2001;8:123–132.
10. Mehta VK, Fisher G, Ford JA, et al. Preoperative chemoradiation for marginally resectable adenocarcinoma of the pancreas. *J Gastrointest Surg.* 2001;5:27–35.
11. Talamonti MS, Small W Jr, Mulcahy MF, et al. A multi-institutional phase II trial of preoperative full-dose gemcitabine and concurrent radiation for patients with potentially resectable pancreatic carcinoma. *Ann Surg Oncol.* 2006;13:150–158.
12. Ishikawa O, Ohhigashi H, Teshima T, et al. Clinical and histopathological appraisal of preoperative irradiation for adenocarcinoma of the pancreatoduodenal region. *J Surg Oncol.* 1989;40:143–151.
13. Lawrence TS, Chang EY, Hahn TM, et al. Radiosensitization of pancreatic cancer cells by 2′,2′-difluoro-2′-deoxycytidine. *Int J Radiat Oncol Biol Phys.* 1996;34:867–872.
14. McGinn CJ, Zalupski MM, Shureiqi I, et al. Phase I trial of radiation dose escalation with concurrent weekly full-dose gemcitabine in patients with advanced pancreatic cancer. *J Clin Oncol.* 2001;19:4202–4208.

15. Ohigashi H, Ishikawa O, Eguchi H, et al. Feasibility and efficacy of combination therapy with preoperative and postoperative chemoradiation, extended pancreatectomy, and postoperative liver perfusion chemotherapy for locally advanced cancers of the pancreatic head. *Ann Surg Oncol.* 2005;12:629–636.
16. Oken MM, Creech RH, Tormey DC, et al. Toxicity and response criteria of the Eastern Cooperative Oncology Group. *Am J Clin Oncol.* 1982;5:649–655.
17. Ishikawa O, Ohigashi H, Sasaki Y, et al. Intraoperative cytodiagnosis for detecting a minute invasion of the portal vein during pancreatoduodenectomy for adenocarcinoma of the pancreatic head. *Am J Surg.* 1998;175:477–481.
18. Ishikawa O, Ohigashi H, Sasaki Y, et al. Liver perfusion chemotherapy via both the hepatic artery and portal vein to prevent hepatic metastasis after extended pancreatectomy for adenocarcinoma of the pancreas. *Am J Surg.* 1994;168:361–364.
19. Ishikawa O, Ohigashi H, Yamada T. Adjuvant regional infusion therapy a: two-channel chemotherapy to prevent hepatic metastasis after extended pancreatectomy for adenocarcinoma of the pancreas: the Osaka experience. In: Evans DB, Pisters PW, Abbruzzese JL, eds. *Pancreatic Cancer.* New York NY: Splinger; 2001:269–274.
20. Evans DB, Rich TA, Byrd DR, et al. Preoperative chemoradiation and pancreaticoduodenectomy for adenocarcinoma of the pancreas. *Arch Surg.* 1992;127:1335–1339.
21. Kaplan E, Meier P. Nonparametric estimation from incomplete observations. *J Am Stat Assoc.* 1958;185:1457–1481.
22. Therasse P, Arbuck SG, Eisenhauer EA, et al. New guidelines to evaluate the response to treatment in solid tumors. European Organization for Research and Treatment of Cancer, National Cancer Institute of the United States, National Cancer Institute of Canada. *J Natl Cancer Inst.* 2000;92:205–216.
23. Ishikawa O, Wada H, Ohigashi H, et al. Postoperative cytology for drained fluid from the pancreatic bed after "curative" resection of pancreatic cancers: does it predict both the patient's prognosis and the site of cancer recurrence? *Ann Surg.* 2003;238:103–110.
24. Spitz FR, Abbruzzese JL, Lee JE, et al. Preoperative and postoperative chemoradiation strategies in patients treated with pancreaticoduodenectomy for adenocarcinoma of the pancreas. *J Clin Oncol.* 1997;15:928–937.
25. Willett CG, Safran H, Abrams RA, et al. Clinical research in pancreatic cancer: the Radiation Therapy Oncology Group trials. *Int J Radiat Oncol Biol Phys.* 2003;56(suppl 4):31–37.
26. Burris HA III, Moore MJ, Andersen J, et al. Improvements in survival and clinical benefit with gemcitabine as first-line therapy for patients with advanced pancreas cancer: a randomized trial. *J Clin Oncol.* 1997;15:2403–2413.
27. Crane CH, Abbruzzese JL, Evans DB, et al. Is the therapeutic index better with gemcitabine-based chemoradiation than with 5-fluorouracil-based chemoradiation in locally advanced pancreatic cancer? *Int J Radiat Oncol Biol Phys.* 2002;52:1293–1302.
28. Ikeda M, Okada S, Tokuuye K, et al. A phase I trial of weekly gemcitabine and concurrent radiotherapy in patients with locally advanced pancreatic cancer. 2002;86:1551–1554.
29. Crane CH, Janjan NA. The stomach and small intestine. In: Cox JD, Ang KK, eds. *Radiation Oncology Rationale Technique Results.* 8th ed. St Louis, MO: Mosby; 2003:444–455.
30. White RR, Hurwitz HI, Morse MA, et al. Neoadjuvant chemoradiation for localized adenocarcinoma of the pancreas. *Ann Surg Oncol.* 2001;8:758–765.
31. Yeung RS, Weese JL, Hoffman JP, et al. Neoadjuvant chemoradiation in pancreatic and duodenal carcinoma. A phase II study. *Cancer.* 1993;72:2124–2133.
32. Foo ML, Gunderson LL, Nagorney DM, et al. Patterns of failure in grossly resected pancreatic ductal adenocarcinoma treated with adjuvant irradiation +/−5 fluorouracil. *Int J Radiat Oncol Biol Phys.* 1993;26:483–489.
33. Hoffman JP, Lipsitz S, Pisansky T, et al. Phase II trial of preoperative radiation therapy and chemotherapy for patients with localized, resectable adenocarcinoma of the pancreas: an Eastern Cooperative Oncology Group Study. *J Clin Oncol.* 1998;16:317–323.
34. Neoptolemos JP, Stocken DD, Friess H, et al. A randomized trial of chemoradiotherapy and chemotherapy after resection of pancreatic cancer. *N Engl J Med.* 2004;350:1200–1210.
35. Oettle H, Post S, Neuhaus P, et al. Adjuvant chemotherapy with gemcitabine vs. observation in patients undergoing curative-intent resection of pancreatic cancer: a randomized controlled trial. *JAMA.* 2007;297:267–277.
36. Yeo CJ, Abrams RA, Grochow LB, et al. Pancreaticoduodenectomy for pancreatic adenocarcinoma: postoperative adjuvant chemoradiation improves survival. A prospective, single-institution experience. *Ann Surg.* 1997;225:621–633; discussion 633–636.
37. Evans DB, Abbruzzese JL, Cleary KR, et al. Preoperative chemoradiation for adenocarcinoma of the pancreas: excessive toxicity of prophylactic hepatic irradiation [comments]. *Int J Radiat Oncol Biol Phys.* 1995;33:913–918.
38. Nakayama S, Takeda S, Kawase Y, et al. Clinical significance of dihydropyrimidine dehydrogenase in adjuvant 5-fluorouracil liver perfusion chemotherapy for pancreatic cancer. *Ann Surg.* 2004;240:840–844.
39. Beger HG, Gansauge F, Buchler MW, et al. Intraarterial adjuvant chemotherapy after pancreaticoduodenectomy for pancreatic cancer: significant reduction in occurrence of liver metastasis. *World J Surg.* 1999;23:946–949.
40. Noda T, Ohigashi H, Ishikawa O, et al. Liver perfusion chemotherapy for selected patients at a high-risk of liver metastasis after resection of duodenal and ampullary cancers. *Ann Surg.* 2007;246:799–805.
41. Shimoyama M, Kimura K. Cytocidal effects of anticancer drugs. In vitro assay with L-1210. *Saisinn Igaku.* 1973;28:1024–1040.

ELSEVIER

Int. J. Radiation Oncology Biol. Phys., Vol. 76, No. 1, pp. 123–129, 2010

0360-3016/10/$–see front matter

doi:10.1016/j.ijrobp.2009.01.038

CLINICAL INVESTIGATION **Esophagus**

FACTORS PREDICTIVE OF TUMOR RECURRENCE AND SURVIVAL AFTER INITIAL COMPLETE RESPONSE OF ESOPHAGEAL SQUAMOUS CELL CARCINOMA TO DEFINITIVE CHEMORADIOTHERAPY

RYU ISHIHARA, M.D.,* SACHIKO YAMAMOTO, M.D.,* HIROYASU IISHI, M.D.,* YOJI TAKEUCHI, M.D.,* NAOTOSHI SUGIMOTO, M.D.,* KOJI HIGASHINO, M.D.,* NORIYA UEDO, M.D.,* MASAHARU TATSUTA, M.D.,* MASAHIKO YANO, M.D.,† ATSUSHI IMAI, M.D.,‡ AND KINJI NISHIYAMA, M.D.‡

Departments of *Gastrointestinal Oncology,† Surgery, and ‡Radiation Oncology, Osaka Medical Center for Cancer and Cardiovascular Diseases, Osaka, Japan

Purpose: To assess factors predictive of recurrent disease and survival after achieving initial complete response (CR) to chemoradiotherapy (CRT) for esophageal cancer.

Methods and Materials: Patients who had clinical Stage I–IVA esophageal cancer and received definitive CRT between 2001 and 2007 were retrospectively analyzed.

Results: Of 269 patients with esophageal cancer, 110 who achieved CR after definitive CRT were included in the analyses. Chemoradiotherapy mainly consisted of 2 cycles of cisplatin and fluorouracil with concurrent radiotherapy of 60 Gy in 30 fractions. We identified 28 recurrences and 28 deaths during follow-up. The cumulative 1- and 3-year recurrence rates were 18% and 32%, respectively. By univariate and multivariate analyses, tumor category (hazard ratio [HR] 6.6; 95% confidence interval [CI] 1.4–30.2; $p = 0.015$) was an independent risk factor for local recurrence, whereas age (HR 3.9; 95% CI 1.1–14.0; $p = 0.034$) and primary tumor location (HR 4.5; 95% CI 1.6–12.4; $p = 0.004$) were independent risk factors for regional lymph node or distant recurrences. The cumulative overall 1- and 3-year survival rates were 91% and 66%, respectively. As expected, recurrence was associated with poor survival ($p = 0.019$). By univariate and multivariate analyses, primary tumor location (HR 3.8; 95% CI 1.2–12.0; $p = 0.024$) and interval to recurrence (HR 4.3; 95% CI 1.3–14.4; $p = 0.018$) were independent factors predictive of survival after recurrence.

Conclusion: Risk of recurrence after definitive CRT for esophageal cancer was associated with tumor category, age, and primary tumor location; this information may help in improved prognostication for these patients. ©2010 Elsevier Inc.

Esophageal cancer, Squamous cell type, Chemoradiotherapy, Complete response, Prognostic factor.

INTRODUCTION

Esophageal cancer is the fifth leading cause of death from cancer worldwide (1). Localized esophageal cancer, regardless of its histologic type, is commonly treated with surgical resection or chemoradiotherapy (CRT), or a combination of both (2–4). Surgical treatment of resectable esophageal cancers results in 5-year survival rates of 5–30%, with higher survival rates in patients with early-stage cancers.

Recent results obtained with CRT in clinical trials support a new standard of care in nonsurgical treatment of potentially curable esophageal cancer. An Intergroup randomized trial, by the Radiation Therapy Oncology Group, of CRT vs. radiotherapy alone showed improved 5-year survival for the combined-modality group (5, 6). An Eastern Cooperative Oncology Group trial showed that CRT provided a better 2-year survival rate than radiotherapy alone (7). With the development of CRT, a surrogate marker of treatment efficacy becomes important. Complete response (CR), defined by clinical disappearance of cancer, is used as an indicator of good response to CRT. Complete response can be achieved in approximately 60% of patients (6, 8), whereas the remaining patients are non-CR. The prognosis of patients who do not obtain CR is often poor, with 2-year survival rates of <10% (8, 9). Although patients with CR are expected to have better prognosis, detailed analysis of the clinical course after CR has not been done. A relatively common clinical problem after CR is the development of local or distant recurrences of cancer, which is observed in 40% of patients who

Reprint requests to: Ryu Ishihara, M.D., Department of Gastrointestinal Oncology, Osaka Medical Center for Cancer and Cardiovascular Diseases, 3-3, Nakamichi 1-chome, Higashinari-ku, Osaka 537-8511, Japan. Tel: (+81) 6-6972-1181; Fax: (+81) 6-6981-4067; E-mail: isihara-ry@mc.pref.osaka.jp

Conflict of interest: none.

Received Sept 25, 2008, and in revised form Jan 17, 2009. Accepted for publication Jan 21, 2009.

achieved CR (3, 6, 8). For effective follow-up and treatment of recurrence, it is important to understand the risk factors and clinical characteristics of recurrence after CR. The study presented here aimed to determine the pattern and timing of recurrences after CR of esophageal cancer and to assess the factors that predict the recurrence and prognosis of recurrent diseases.

METHODS AND MATERIALS

Patient population

The medical records of patients who underwent CRT for esophageal cancer in our institution between January 2001 and October 2007 were retrospectively reviewed. Only patients who had clinical Stage I–IVA (modified International Union Against Cancer [UICC] tumor–node–metastasis system, 1997) cancer and who obtained CR after definitive CRT were included in the analysis. Patients were excluded if they were treated with combination therapy of CRT and operation or CRT and endoscopic resection. Patients were also excluded if they could not receive a sufficient dose of RT (≥50 Gy) or chemotherapy (more than half of planned dose) or if they did not have a follow-up examination. Informed consent to perform CRT was obtained from all patients.

Pretreatment evaluation and modified UICC staging system

Pretreatment evaluations included barium tests, esophageal endoscopy, and CT of the neck, chest, and abdomen. Endosonography of the esophagus, bronchoscopy, ultrasound evaluation of the neck, and positron emission tomography scans were optional. Tumor locations were classified into cervical esophagus, upper thoracic esophagus, middle thoracic esophagus, and lower thoracic esophagus. In this study we used a modified UICC staging system, whereby the T category was determined by endoscopy and CT. The criteria for endoscopic evaluation of the T category were based on the Japanese Classification of Esophageal Cancer as proposed by the Japanese Esophageal Society (10). The typical endoscopic appearance of each tumor category (11, 12) is shown in Table 1. Lymph nodes were classified as N1 if the maximal transverse diameter of these nodes was >1 cm.

Treatment details

A total of 103 patients were treated with cisplatin and fluorouracil–based chemotherapy. The most frequently used treatment protocol consisted of cisplatin, at a dose of 70 mg/m^2 body surface area, and was given as a rapid intravenous infusion after prehydration on Day 1. Fluorouracil was administered at a dose of 700 mg/m^2 body surface area as a continuous infusion from Day 1 through Day 4 (96 h). The second cycle of chemotherapy was repeated from the day of the 21st radiation fraction. Five patients with renal dysfunction (serum creatinine level 1.3–1.5 mg/dL) were treated by nedaplatin and fluorouracil. Two patients with poor performance status were treated with low-dose docetaxel (10 mg/m^2 weekly).

Concurrent radiotherapy using 10-MV X-rays was delivered at a dose of 2 Gy per day, 5 days per week, for a total dose of 60 Gy in 30 fractions. A break of 2 weeks was planned after the administration of 30 Gy from January 2001 to September 2004, but from October 2004 the total dose was delivered without a planned break. The initial 40 Gy was delivered through anterior–posterior opposed portals, and the following 20 Gy was given through right-anterior and left-posterior opposed portals excluding the spinal cord. The dose was prescribed to the isocenter at the middle of the planned target volume. In patients with Stage I cancer, the planned target volume was defined by adding 2–3-cm margins in a longitudinal direction and a 1-cm margin radially to each side of the primary esophageal tumor. In patients assessed as Stages II–IVA, except T4 cases, 40 Gy in 4 weeks was delivered to the regional lymph nodes as well as the primary esophageal tumor and the metastatic lymph nodes. The regional lymph node areas were from the supraclavicular to the upper mediastinal area in cervical esophageal cancer, from the supraclavicular to the mid-mediastinal area in upper thoracic esophageal cancer, from the supraclavicular to the periceliac area in middle thoracic esophageal cancer, and from the upper mediastinal to the periceliac area in lower thoracic esophageal cancer. An additional 20 Gy in 2 weeks was given to the esophageal tumor and the metastatic lymph nodes as a booster dose. In some cases, however, the targets were shrunk on the basis of the patient's condition or the physician's judgment. In patients with T4 cancer, a total dose of 60 Gy was given to the target of the gross esophageal mass and enlarged lymph nodes. The margins for gross tumor volume were similar to those in patients with Stage I cancer. In patients with Stage II–IVA cancer, an additional 2 cycles of cisplatin and fluorouracil were administered at the same doses for responders every 4–6 weeks.

Table 1. Endoscopic appearance of each T category

T category	Endoscopic appearance
T1	Slightly elevated or depressed tumors, usually with red appearance and an irregular surface. If the tumors are protruded, they are supple with a narrow base and sometimes pedunculated. If the tumors are ulcerated, they have only shallow ulcers.
T2, T3	Large and tall tumors, usually with a broad base. Deep ulcerated tumors with stiffening and irregular tumorous bank, sometimes with circular stenosis. Differentiation between T2 and T3 is based on the depth of ulceration, extension of the lesion, and degree of stenosis.
T4	Tumors with invasion of any neighboring structure that is identified by CT scan or other staging modality.

Response assessment

Complete response for the primary tumor was defined upon endoscopic observation of the entire esophagus as disappearance of the tumor lesion, ulceration, and absence of cancer cells in biopsy specimens. The existence of a granular protruded lesion or iodine-unstained area did not prevent application of the primary CR criteria (9, 10). Complete response for lymph nodes was defined according to the Response Evaluation Criteria in Solid Tumors guideline (13) as the complete disappearance of the lymph nodes. However, lymph nodes of <5 mm or residual connective tissue after disappearance of cancer with no evidence of progression after completion of treatment were regarded as noncancerous tissue. These findings did not prevent application of CR.

Follow-up evaluation and pattern of recurrence

Follow-up evaluations were performed 1 month after CRT and then every 3–6 months for the first 2 years and every 6 months thereafter. Each evaluation included a physical examination, blood test, endoscopy of the esophagus, and CT scan of the neck, chest, and abdomen. Biopsy of the primary tumor site was performed when

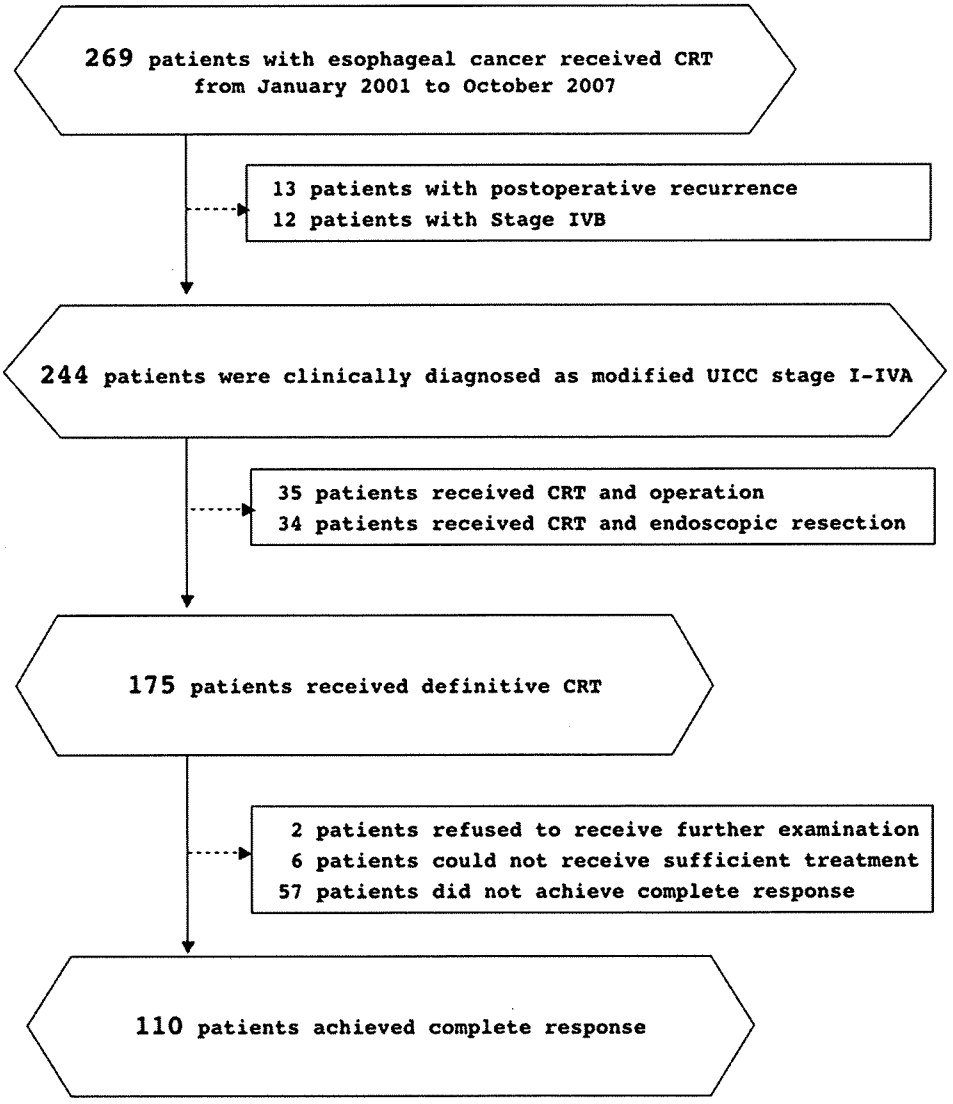

Fig. 1. Flow chart of patient recruitment. CRT = chemoradiotherapy; UICC = International Union Against Cancer.

abnormal findings were detected in the esophagus. Patterns of treatment failure were defined as the first site of recurrence. Local recurrence included the primary tumor. Regional recurrence included regional lymph nodes. Distant recurrence included any site beyond the primary tumor and regional lymph nodes. Regional and distant recurrence was further defined as non-local recurrence. When metastasis was observed in patients with a second primary cancer other than at the esophagus, the origin of metastasis was decided on the basis of the histology and/or distribution of metastatic cancer.

Statistical analysis

For analysis, the start of follow-up was defined as Day 1 of CRT, and the end was either the date of death or May 1, 2008, whichever occurred first. Time to recurrence was calculated from the day CRT was started to the time of recurrence. Survival after recurrence was calculated from the time of recurrence to the end of follow-up. Kaplan-Meier curves were constructed for analyses of survival and recurrence. Log–rank tests were used to evaluate the statistical significance of differences. Because of the small number of patients who met each endpoint, we needed to limit variables for multivariate analysis. Therefore, independent factors were determined by Cox's regression hazard model using the variables that had significant or marginally significant differences on univariate analysis. For all analyses a two-sided p value of ≤ 0.05 was considered statistically significant. All analyses were performed in accordance with the ethical standards of the institutional review board using StatView 5.0 (SAS Institute, Cary, NC) on a personal computer.

RESULTS

Patient characteristics

A flow chart of patient recruitment is shown in Fig. 1. From January 2001 to October 2007, 269 patients with esophageal cancer received CRT. Of these, 175 patients with modified UICC Stage I–IVA disease received definitive CRT as their first treatment. Overall, 110 (64%) of 173 patients who received follow-up examination were confirmed to have achieved CR. Of 173 esophageal cancers treated, 47 cancers (T4 in 26 patients [55%], N1 in 32 patients [68%]) were above the tracheal bifurcation, whereas 126

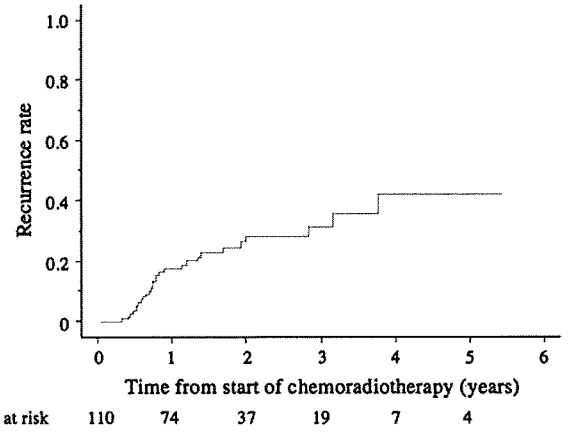

Fig. 2. Recurrence rate among patients achieving complete response. Of 110 patients, 28 had recurrent diseases. The cumulative 1- and 3-year recurrence rates were 18% and 32%, respectively. Median time to recurrence from chemoradiotherapy was 9 months (range, 4–47 months), with 82% (23 of 28) of all recurrences developing within 21 months of chemoradiotherapy.

cancers (T4 in 30 patients [24%], N1 in 45 patients [36%]) were lower than the tracheal bifurcation.

The characteristics of the patients who achieved CR were as follows. The median (range) age was 65 (42–86) years. There were 95 men and 15 women. Performance status was 0 in 94 patients and 1 in 16 patients. All of the tumors were squamous cell carcinoma. The T category before treatment was T1 in 64 patients, T2 in 14 patients, T3 in 15 patients, and T4 in 17 patients. The N category before treatment was N1 in 30 patients and N0 in 80 patients. The location of primary tumor was cervical esophagus in 4 patients, upper thoracic esophagus in 22 patients, middle thoracic esophagus in 62 patients, and lower thoracic esophagus in 22 patients.

Recurrence and its treatment

A total of 28 patients were found to have recurrent disease. The cumulative 1- and 3-year recurrence rates were 18% and 32%, respectively (Fig. 2). Local recurrences were recognized in 13 patients (12%), regional recurrence in 7 (6%; cervical in 2, mediastinal in 4, and abdominal in 1), and distant recurrences in 8 (7%; nonregional lymph node in 3, lung in 3, liver in 1, and cerebral in 1). Lymph node metastasis in 1 patient and lung metastasis in another developed within 2 months after local recurrences. However, these patients were regarded as local recurrence, because patterns of treatment failure were defined as the first site of recurrence. All of the local recurrences and two of the non-local recurrences occurred in areas inside the radiation field. Eleven (73%) of the 15 non-local recurrences occurred in areas outside the radiation field. The other two non-local recurrences occurred in a borderline area. Local recurrences mainly originated from T2–T4 cancer (85%; 11 of 13 patients), whereas non-local recurrences mainly originated from cervical or upper thoracic esophageal cancer (53%; 8 of 15 patients). Median (range) time to recurrence from CRT was 9 (4–47) months, whereas 82% (23 of 28) of all recurrences developed within 21 months of CRT. The median time to local recurrence was 9 (5–39) months, and the median time to non-local recurrence was 10 (4–47) months.

Of the 28 patients who had recurrence, 15 had received potentially curative treatment. Five patients with local recurrence and 5 with regional lymph node or brain metastasis underwent surgery. Four patients with local recurrence received endoscopic treatment (endoscopic resection in 2, photodynamic therapy in 2). One patient with regional recurrence received chemoradiotherapy. Of the 15 patients, 8 were successfully treated without further recurrence.

The other 13 patients had received palliative treatment. Two patients with local recurrence and 8 with non-local recurrence received palliative chemotherapy. One patient with dysphagia because of local recurrence was palliated with a stent insertion. One patient with local recurrence and 1 with regional lymph node recurrence had no specific treatment other than pain control. Of the 28 patients with recurrence, 13 died from the recurrence, and 1 died of heart disease during follow-up.

Survival

All 110 patients (100%) were completely followed up until their death or May 1, 2008, with a mean (range) observation period of 21 (4–67) months. We identified 28 deaths during the follow-up period. Death from esophageal cancer was identified in 13 of these. Death from malignant tumor other than esophageal cancer was identified in 6 patients. One patient with a malignant tumor was diagnosed before, and 3 were diagnosed together with, and the other 2 were diagnosed after the diagnosis of esophageal cancer. The origin of the malignant tumors was the liver in 2 patients, and mesopharynx, tongue, colon, and kidney in 1 each. Other causes of death were radiation pneumonitis possibly related to CRT in 3 patients, bacterial pneumonia in 2 patients, heart disease in 2, pleural effusion possibly related to CRT in 1, and cirrhosis in 1.

The cumulative overall 1- and 3-year survival rates were 91% and 66%, respectively. The cumulative disease-free 1- and 3-year survival rates were 77% and 55%. Stratification of survival according to the existence of recurrence confirmed a significantly worse survival for patients with recurrence ($p = 0.019$) (Fig. 3). The median survival of patients with recurrence was 36 months and without was 63 months. The median survival after detection of recurrent esophageal carcinoma was 20 months (Fig. 4).

Factors predicting recurrence and survival after recurrence

Risk factors for local and non-local recurrence were assessed separately. By univariate analysis, local recurrence was predicted by T category and non-local recurrence was predicted by patient age and primary tumor location (Table 2). By multivariate analysis for local recurrence, T category was an independent risk factor, whereas planned interruption of radiation was not independently associated (Table 3). By

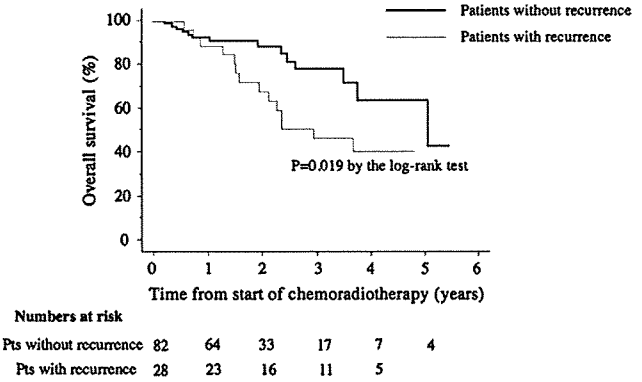

Fig. 3. Overall survival of patients with or without recurrence after achieving complete response. Stratification of survival according to the existence of recurrence confirmed significantly worse survival for patients with recurrence ($p = 0.019$). Median survival of patients with recurrence was 36 months, but 63 months for patients without.

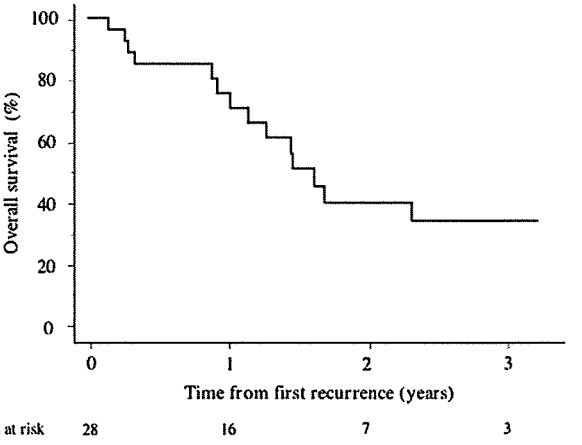

Fig. 4. Overall survival of patients with recurrence from the date of first recurrence. Fourteen patients died during follow-up. The median survival after detection of recurrent esophageal carcinoma was 20 months (range, 2–38 months).

multivariate analysis for non-local recurrence, age and primary tumor location were again confirmed to be independent factors (Table 4). When local and non-local recurrences were assessed together, T category ($p = 0.02$), primary tumor location ($p = 0.004$), and age ($p = 0.06$) were significant or marginally significant factors for recurrence. Primary tumor location (hazard ratio 2.4; 95% confidence interval 1.1–5.3; $p = 0.03$) was confirmed to be an independent factor.

By univariate analysis, survival after recurrence was predicted by primary tumor location and the interval to recurrence (Table 5). By multivariate analysis, primary tumor location and interval to recurrence were again confirmed as independent predictive factors for survival (Table 6). Multivariate analysis was performed with limited variables because some groups might have no patient when other variables were added into the analysis.

Table 2. Risk factors for recurrence (univariate analysis)

Subgroup	Patients (*n*)	Local recurrence (%)	*p*	Non-local recurrence (%)	*p*
Age (y)			0.801		0.022
<65	54	7 (13)		12 (22)	
≥65	56	6 (11)		3 (5)	
Gender			0.132		0.605
Male	95	13 (14)		13 (14)	
Female	15	0		2 (13)	
Performance status			0.946		0.079
0	94	11 (12)		15 (16)	
1	16	2 (13)		0	
T category (1)			0.002		0.777
T1	64	2 (3)		8 (13)	
T2–4	46	11 (24)		7 (15)	
T category (2)			0.136		0.706
T1–3	93	9 (10)		13 (14)	
T4	17	4 (24)		2 (12)	
N category			0.194		0.332
N0	80	8 (10)		10 (13)	
N1	30	5 (17)		5 (17)	
Primary tumor location			0.423		0.002
Ce, Ut	26	4 (15)		8 (31)	
Mt, Lt	84	9 (11)		7 (8)	
Chemotherapeutic regimen			0.785		0.347
FP-based	103	12 (12)		15 (15)	
Non–FP-based	7	1 (14)		0	
Radiation schedule			0.064		0.763
With planned interruption	34	8 (24)		7 (21)	
Without planned interruption	76	5 (7)		8 (11)	

Abbreviations: Ce = cervical esophagus; Ut = upper thoracic esophagus; Mt = middle thoracic esophagus; Lt = lower thoracic esophagus; FP = cisplatin and fluorouracil.

Table 3. Risk factors for local recurrence (multivariate analysis)

Subgroup	Patients (*n*)	HR (95% CI)	*p*
T category			0.015
T1 (reference)	64	1	
T2–4	46	6.6 (1.4–30.2)	
Radiation schedule			0.200
Without planned interruption (reference)	76	1	
With planned interruption	34	2.1 (0.7–6.8)	

Abbreviations: HR = hazard ratio; CI = confidence interval.

DISCUSSION

Tumor recurrence was observed in 28 patients with a median follow-up of 21 months. The risk factor for local recurrence was T2–T4 cancer. For non-local recurrence, the risk factors were cervical or upper thoracic esophageal cancer, and age <65 years. Early recurrence and recurrence from cervical or upper thoracic esophageal cancer were adverse predictors of survival.

Non-local recurrence occurred frequently from cancers of cervical and upper thoracic esophageal origin. Aggressive characteristics and a worse survival rate have been reported for cancer of the upper esophagus (14). Upper esophageal cancer located above the tracheal bifurcation is more often diagnosed in advance stages (higher prevalence of T4 disease and higher cervical lymph node metastasis) (15, 16). In accordance with these reports, at presentation the upper esophageal cancers in our study had a higher prevalence of T4 and N1 disease (55% and 68%, respectively) compared with middle or lower esophageal cancers (24% and 36%). These aggressive characteristics of cervical and upper thoracic esophageal cancer may result in a higher rate of micrometastasis, which is related to non-local recurrence. Denham *et al.* (17) reported that upper esophageal cancer was more sensitive to CRT and had better prognosis. Our study should be interpreted considering the differences in the two studies. Our study included patients with cervical esophageal cancer and more cases of T4 cancer in the upper esophagus.

The strongest adverse predictor for survival after recurrence was the timing of recurrence from the starting date of CRT. Recurrence of cancer basically originates from micro-residues of cancer cells at the local or other sites. An excess volume of residual cancer cells may cause early recurrence, leading to a poor prognosis. The characteristics of the cancer itself may also differ among esophageal cancer patients, and this will affect survival after recurrence. Cancers with higher proliferative potential will show fast regrowth after completion of CRT, which may cause early recurrence along with poor prognosis. Thus, in our opinion, the poor prognoses of early-recurrent cancers can be explained by excess volume of residual cancer or the higher proliferative potential of these cancers.

A limitation of this study is the short follow-up period. The median follow-up of 21 months might be seen as too short for survival analysis. However, considering that the median time

Table 4. Risk factors for non-local recurrence (multivariate analysis)

Subgroup	Patients (*n*)	HR (95% CI)	*p*
Age (y)			0.034
≥65 (reference)	56	1	
<65	54	3.9 (1.1–14.0)	
Primary tumor location			0.004
Mt, Lt (reference)	84	1	
Ce, Ut	26	4.5 (1.6–12.4)	

Abbreviations as in Tables 2 and 3.

Table 5. Predictors of survival after recurrence (univariate analysis)

Subgroup	Patients (*n*)	Median survival (d)	*p*
Age (y)			0.46
<65	19	535	
≥65	9	595	
Gender			0.97
Male	26	537	
Female	2	618	
Performance status (before CRT)			0.19
0	26	618	
1	2	345	
Performance status (recurrence)			0.15
0	22	618	
1	6	102	
T category (before CRT) (1)			0.14
T1	10	>1179	
T2–4	18	466	
T category (before CRT) (2)			0.53
T1–3	22	537	
T4	6	>1073	
N category (before CRT)			0.11
N0	18	850	
N1	10	537	
Primary tumor location			0.043
Ce, Ut	12	422	
Mt, Lt	16	1091	
Recurrent site			0.81
Local	13	595	
Non-local	15	537	
Interval to recurrence			0.025
Early (<9 mo)	14	422	
Late (≥9 mo)	14	>1179	

Abbreviation: CRT = chemoradiotherapy. Other abbreviations as in Tables 2 and 3.

Table 6. Predictors of survival after recurrence (multivariate analysis)

Subgroup	Patients (*n*)	HR (95% CI)	*p*
Primary tumor location			0.024
Mt, Lt (reference)	16	1	
Ce, Ut	12	3.8 (1.2–12.0)	
Interval to recurrence			0.018
Late (≥9 mo) (reference)	14	1	
Early (<9 mo)	14	4.3 (1.3–14.4)	

Abbreviations as in Tables 2 and 3.

to recurrence was 9 months and more than 80% of recurrences occurred within 21 months, our follow-up period was not too short for our analysis. We could at least detect significant risk factors for recurrence and prognostic factors for survival after recurrence.

To improve the survival rate after recurrence, an effective follow-up system for patients who achieve CR needs to be established. Given that 20 of the 28 cases of recurrence occurred at a local site or at a regional lymph node, early detection would enable curative salvage treatment to be undertaken. In this study, we identified possible risk factors for recurrence after CRT. Stratification of patients by the risk of recurrence enables the effective performance of patient follow-up. Intensive follow-up of high-risk patients would contribute to the earlier detection of recurrence and thus improved survival after recurrence. The utility of endosonography compared with CT or endoscopy in the assessment of residual cancer after CRT has been reported (18, 19). Endosonography can detect small lymph nodes or small submucosal lesions that are undetectable by CT or endoscopy. By observing changes in size, we can differentiate recurrence from other lesions. Because approximately two thirds of recurrences were detected within 1 year after CRT, the efficacy of intensive follow-up of high-risk patients for at least 1 year with endosonography should be evaluated in future studies.

At the same time, modification of treatment strategies to avoid recurrence should also be considered, because earlier detection of recurrence is not always possible. The addition of more-aggressive chemotherapy or local treatment after CRT would reduce recurrence for patients at high risk of recurrence. The efficacy of photodynamic therapy as a rescue therapy for local recurrent or persistent cancer after chemoradiotherapy has been reported (20). Therefore, the combined treatment of CRT followed by photodynamic therapy might improve local control of esophageal cancer. According to the results of the present study, T2–T4 cancer may be a good candidate for such a treatment strategy.

CONCLUSIONS

Of 110 patients with esophageal cancer who achieved CR after definitive CRT, tumor recurrence was observed in 28 patients with a median follow-up of 21 months. Local recurrence was associated with the T category, whereas non-local recurrence was associated with patient age and primary tumor location. Stratification of survival by the existence of recurrence confirmed significantly worse survival for patients with recurrence. This information may help in improving prognostication in these patients. To improve survival after recurrence, follow-up using another modality, such as endosonography, should be considered for patients at higher risk of recurrence.

REFERENCES

1. World Health Organization. The world health report 1997. Geneva: WHO; 1997.
2. Enzinger PC, Mayer RJ. Esophageal cancer. *N Engl J Med* 2003;349:2241–2252.
3. Minsky BD, Pajak TF, Ginsberg RJ, *et al.* INT 0123 (Radiation Therapy Oncology Group 94-05) phase III trial of combined-modality therapy for esophageal cancer: High-dose versus standard-dose radiation therapy. *J Clin Oncol* 2002;20:1167–1174.
4. Stahl M, Stuschke M, Lehmann N, *et al.* Chemoradiation with and without surgery in patients with locally advanced squamous cell carcinoma of the esophagus. *J Clin Oncol* 2005;23:2310–2317.
5. Herskovic A, Martz K, al-Sarraf M, *et al.* Combined chemotherapy and radiotherapy compared with radiotherapy alone in patients with cancer of the esophagus. *N Engl J Med* 1992;326:1593–1598.
6. Cooper JS, Guo MD, Herskovic A, *et al.* Chemoradiotherapy of locally advanced esophageal cancer: Long-term follow-up of a prospective randomized trial (RTOG 85-01). Radiation Therapy Oncology Group. *JAMA* 1999;281:1623–1627.
7. Smith TJ, Ryan LM, Douglass HO Jr., *et al.* Combined chemoradiotherapy vs. radiotherapy alone for early stage squamous cell carcinoma of the esophagus: A study of the Eastern Cooperative Oncology Group. *Int J Radiat Oncol Biol Phys* 1998;42:269–276.
8. Ishikura S, Nihei K, Ohtsu A, *et al.* Long-term toxicity after definitive chemoradiotherapy for squamous cell carcinoma of the thoracic esophagus. *J Clin Oncol* 2003;21:2697–2702.
9. Tahara M, Ohtsu A, Hironaka S, *et al.* Clinical impact of criteria for complete response (CR) of primary site to treatment of esophageal cancer. *Jpn J Clin Oncol* 2005;35:316–323.
10. Japan Esophageal Society. Japanese classification of esophageal cancer. 10th ed. Tokyo: Kanehara; 2008.
11. Dittler HJ, Pesarini AC, Siewert JR. Endoscopic classification of esophageal cancer: Correlation with the T stage. *Gastrointest Endosc* 1992;38:662–668.
12. Kienle P, Buhl K, Kuntz C, *et al.* Prospective comparison of endoscopy, endosonography and computed tomography for staging of tumours of the oesophagus and gastric cardia. *Digestion* 2002;66:230–236.
13. Therasse P, Arbuck SG, Eisenhauer EA, *et al.* New guidelines to evaluate the response to treatment in solid tumors. European Organization for Research and Treatment of Cancer, National Cancer Institute of the United States, National Cancer Institute of Canada. *J Natl Cancer Inst* 2000;92:205–216.
14. Law S, Kwong DL, Kwok KF, *et al.* Improvement in treatment results and long-term survival of patients with esophageal cancer: Impact of chemoradiation and change in treatment strategy. *Ann Surg* 2003;238:339–347.
15. Vigneswaran WT, Trastek VF, Pairolero PC, *et al.* Extended esophagectomy in the management of carcinoma of the upper thoracic esophagus. *J Thorac Cardiovasc Surg* 1994;107:901–906.
16. Isono K, Sato H, Nakayama K. Results of a nationwide study on the three-field lymph node dissection of esophageal cancer. *Oncology* 1991;48:411–420.
17. Denham JW, Steigler A, Kilmurray J, *et al.* Relapse patterns after chemo-radiation for carcinoma of the oesophagus. *Clin Oncol (R Coll Radiol)* 2003;15:98–108.
18. Nousbaum JB, Robaszkiewicz M, Cauvin JM, *et al.* Endosonography can detect residual tumour infiltration after medical treatment of oesophageal cancer in the absence of endoscopic lesions. *Gut* 1992;33:1459–1461.
19. Agarwal B, Swisher S, Ajani J, *et al.* Endoscopic ultrasound after preoperative chemoradiation can help identify patients who benefit maximally after surgical esophageal resection. *Am J Gastroenterol* 2004;99:1258–1266.
20. Yano T, Muto M, Minashi K, *et al.* Photodynamic therapy as salvage treatment for local failures after definitive chemoradiotherapy for esophageal cancer. *Gastrointest Endosc* 2005;62:31–36.

ELSEVIER

Int. J. Radiation Oncology Biol. Phys., Vol. 75, No. 2, pp. 543–548, 2009

0360-3016/09/$–see front matter

doi:10.1016/j.ijrobp.2008.12.091

5TH JUCTS AND THE 5TH S. TAKAHASHI MEMORIAL INTERNATIONAL JOINT SYMPOSIUM

MEASUREMENT OF INTERFRACTION VARIATIONS IN POSITION AND SIZE OF TARGET VOLUMES IN STEREOTACTIC BODY RADIOTHERAPY FOR LUNG CANCER

KIYOTOMO MATSUGI, M.S.,* YUICHIRO NARITA, PH.D.,* AKIRA SAWADA, PH.D.,* MITSUHIRO NAKAMURA, M.S.,* YUKI MIYABE, M.S.,* YUKINORI MATSUO, M.D., PH.D.,* MASARU NARABAYASHI, M.D.,* YOSHIKI NORIHISA, M.D.,* TAKASHI MIZOWAKI, M.D., PH.D.,* AND MASAHIRO HIRAOKA, M.D., PH.D.*

*Department of Radiation Oncology and Image-Applied Therapy, Kyoto University Graduate School of Medicine, Kyoto, Japan

Purpose: To investigate the interfraction variations in volume, motion range, and position of the gross tumor volume (GTV) in hypofractionated stereotactic body radiotherapy (SBRT) for lung cancer using four-dimensional computed tomography.

Methods and Materials: Four-dimensional computed tomography scans were acquired for 8 patients once at treatment planning and twice during the SBRT period using a stereotactic body frame. The image registration was performed to correct setup errors for clinical four-dimensional computed tomography. The interfraction variations in volume, motion range, and position of GTV were computed at end-inhalation (EI) and end-exhalation (EE).

Results: The random variations in the GTV were 0.59 cm^3 at EI and 0.53 cm^3 at EE, and the systematic variations were 3.04 cm^3 at EI and 3.21 cm^3 at EE. No significant variations in GTV were found during the SBRT sessions ($p = .301$ at EI and $p = .081$ at EE). The random variations in GTV motion range for the upper lobe in the craniocaudal direction were within 1.0 mm and for the lower lobe was 3.4 mm. The interfraction variations in the GTV centroid position in the anteroposterior and craniocaudal directions were mostly larger than in the right–left direction; however, no significant displacement was observed among the sessions in any direction.

Conclusion: For patients undergoing hypofractionated SBRT, interfraction variations in GTV, motion range, and position mainly remained small. An additional approach is needed to assess the margin size. © 2009 Elsevier Inc.

Stereotactic body radiotherapy, SBRT, four-dimensional computed tomography, 4D-CT, interfraction variations.

INTRODUCTION

Stereotactic radiotherapy (RT), which delivers a high dose to a target with a high degree of precision, has been established for intracranial lesions, and the application has been expanded to extracranial tumors such as lung and liver cancer (1–4). Hypofractionated stereotactic body RT (SBRT) provides a shorter irradiation period than conventional RT. However, target mispositioning will result in a high radiation dose to the normal tissues and an insufficient dose to the target.

Traditionally, the planning target volume (PTV) is defined as the clinical target volume with a safety margin that includes the target internal motion and daily setup error (5). Some researchers have reported that the tumor position varies interfractionally (6), as well as intrafractionally (7). Therefore, accurate measurement of the tumor motion for an individual patient would help in determining the patient-specific margin sizes.

Respiratory-correlated or four-dimensional computed tomography (4D-CT) is a powerful tool for estimating tumor motion. Several studies have demonstrated intrafraction and interfraction lung tumor motion with respiratory-correlated or 4D-CT during conventional RT (8–13). 4D-CT not only images the respiratory motion of tumors and organs at risk but can also reduce motion artifacts.

Significant regression in lung tumor volume can occur by 3 weeks after beginning treatment (8–10). The interfraction baseline tumor variations have been large (11), but no time trend in the tumor motion range was observed (8, 9, 11, 12). However, few investigations of the interfraction variations in tumor volume and motion on hypofractionated SBRT with respiratory-correlated or 4D-CT have been described. High-dose delivery per fraction might result in greater variations in the tumor volume and motion during hypofractionated SBRT compared with those occurring with conventional RT. We measured the interfraction variations

Reprint requests to: Yuichiro Narita, Ph.D., Department of Radiation Oncology and Image-Applied Therapy, Graduate School of Medicine, Kyoto University, Kyoto, Japan. Tel: (+81) 75-751-3762; Fax: (+81) 75-771-9747; E-mail: ynrt@kuhp.kyoto-u.ac.jp

Partly supported by a Grant-in-Aid for Scientific Research from the Ministry of Education, Culture, Sports, Science and Technology of Japan (Grant 20229009).

Conflict of interest: none.

Received Sept 30, 2008, and in revised form Dec 8, 2008. Accepted for publication Dec 8, 2008.

in volume, motion range, and position of the gross tumor volume (GTV) in hypofractionated SBRT for lung cancer using 4D-CT.

METHODS AND MATERIALS

Patients

A total of 8 patients, who provided written informed consent, were enrolled in the present study. The institutional review board approved the study protocol. The patient characteristics are listed in Table 1. Each patient had primary or metastatic lung cancer with a diameter of not >4 cm. X-ray fluoroscopic examination, slow CT scan with a rotation time of 4 s, and 4D-CT images were used to determine the internal target volume (13). The PTV was generated by adding 5-mm margins to the internal target volume in the right–left (RL), anteroposterior (AP), and craniocaudal (CC) directions. The patients received a prescription dose of 48 Gy for primary lung cancer or 56 Gy for metastatic lung cancer at the isocenter in four fractions within 1 week.

CT acquisition

Four-dimensional CT data sets were acquired with a LightSpeed RT scanner (GE Healthcare, Milwaukee, WI), and the respiratory motion was obtained with a real-time position management respiratory gating system (Varian Oncology System, Palo Alto, CA). Each patient was firmly fixed using a stereotactic body frame (SBF) immobilization system (Elekta, Stockholm, Sweden) (14). One respiratory cycle in a 4D-CT data set was divided into eight phases (0% indicates end-inhalation [EI] and 50%, end-exhalation [EE]) and sorted to reconstruct the corresponding phase images using Advantage4D software (GE Healthcare) (15).

The 4D-CT scans were acquired once at treatment planning (Session 1) and twice (Sessions 2 and 3) during treatment under free-breathing conditions. The interval between Sessions 1 and 2 and Sessions 2 and 3 for 4D-CT acquisition was 5–14 and 2 days, respectively. Sessions 2 and 3 were on the second and last day of the treatment course for 7 patients and was the first and second day for 1 patient, respectively. Thus, 24 4D-CT data sets were investigated. In Session 1, the 4D-CT images were acquired for the whole lung. In contrast, in Sessions 2 and 3, the scanning range was limited to around the tumor (from 7.5 cm to 10.0 cm) to reduce exposure to the normal tissue.

Three-dimensional image registration using bony anatomy projection patterns

The setup errors between Session 1 and the other sessions were measured using an in-house image registration technique based on the bony anatomy projection patterns. First, phase-averaged images among the adjacent five phase images centered at EE were computed to avoid motion artifacts on 4D-CT. Next, each phase-averaged image was thresholded by a predetermined CT value of 160 Hounsfield units to extract the bony regions. Subsequently, voxels marked as the bony region in the orthogonal plane to the RL direction were counted to generate projection patterns of the bony voxels as a function of position in the RL direction. This was also done for the AP and CC directions (Fig. 1). During the translation and rotation of the images in Sessions 2 and 3, the sums of the absolute difference in values between the projection patterns in Session 1 and Sessions 2 and 3 for each position were iteratively minimized.

Our registration technique was verified using a thorax phantom with seven steel markers. Initially, a reference three-dimensional CT scan was acquired with the phantom placed at the initial position.

Table 1. Patient characteristics

Pt. No.	Age (y)	Gender	Clinical stage	Histologic type	Tumor location	Tumor size (mm)
1	69	Female	T1N0M0	S	RUL	15
2	63	Male	T1N0M0	L or S	LUL	28
3	83	Male	T1N0M0	U	RUL	30
4	84	Female	T1N0M0	S	RUL	20
5	77	Male	T1N0M0	A	RLL	13
6	77	Female	T1N0M0	A	RLL	19
7	78	Male	T1N0MX	S	RLL	25
8	78	Male	M1	A	RLL	25

Abbreviations: S = squamous cell carcinoma; RUL = right upper lobe; L = large cell neuroendocrine carcinoma; LUL = left upper lobe; U = unknown; A = adenocarcinoma; RLL = right lower lobe.

Subsequently, the phantom position was varied by a translation pixel range of ±10 mm for each direction and a rotation angle range of ±2° around each axis. Next, three-dimensional CT images, "moved images," were acquired by choosing a translation amount and rotation angle. This procedure was repeated using six combinations of the translation and rotation amounts. Next, our registration method was performed for the reference and moved images. The registration results were compared with the positional differences of the measured steel markers in each direction to calculate the residual error.

Analysis of tumor volume variations

All GTVs were contoured using a pulmonary window setting (window level, −700 Hounsfield units and window width, 2,000 Hounsfield units) in each respiratory phase image using the Eclipse treatment planning system (Varian Oncology Systems) by a medical physicist (M.N.) and were reviewed by an experienced radiation oncologist (Y.M.). The volumes and centroid positions of the GTV were calculated in the treatment planning system. The interfraction variations in volume, motion range, and centroid position of the GTV were computed for images at EI and EE, which contained fewer motion artifacts. The motion range was defined as the distance between GTV centroid position at EE and EI. The group mean (GM), Σ, and σ were calculated at EI and EE for the analysis. Σ is the standard deviation (SD) of the mean GTV centroid position (systematic variation), and σ is interfraction variation, defined as the root

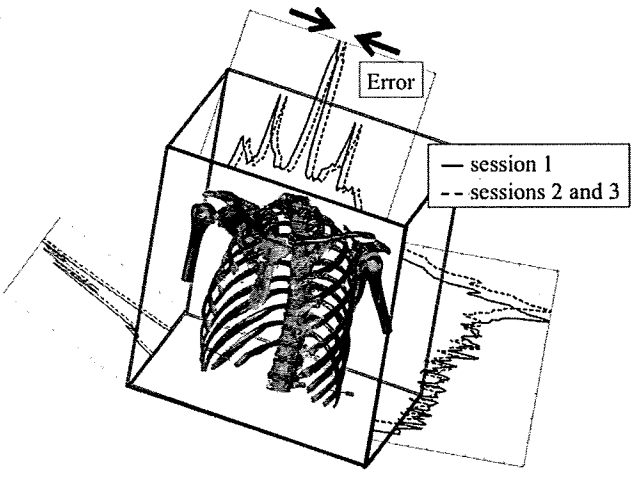

Fig. 1. Illustration of three-dimensional image registration using bony anatomy projection patterns.

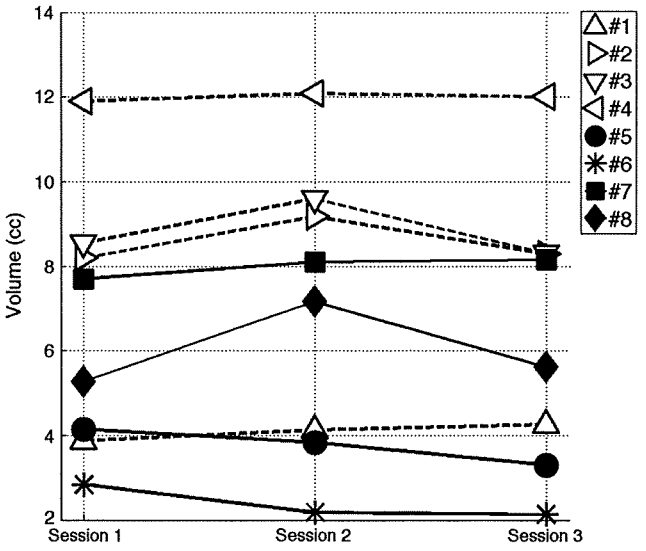

Fig. 2. Interfraction variations in gross tumor volume at end-exhalation among three sessions. Dashed lines indicate variations for upper lobe tumors; solid lines, variations for lower lobe tumors. No significant variations were seen among three sessions at end-inhalation (p = .301) or end-exhalation (p = .081).

mean square of the SD in the GTV centroid position (random variation) per patient. Also, the internal GTV (iGTV) was defined as the combined volume of all GTVs. Subsequently, the interfraction variations in volume and the centroid position of iGTV were computed.

Statistical analysis

The interfraction variations in the GTV at EI and EE and those in motion range for each direction among the sessions were statistically analyzed using repeated measures analysis of variance with the two independent factors of patients and sessions. One-way analysis of variance was performed with the factors of patients and sessions to compare the interfraction displacement of the GTV centroid position for each direction among the sessions. Differences in the RL, AP, and CC directions were tested by one-way analysis of variance and Tukey's test. Differences for the upper and lower lobes were tested using Student's t test.

RESULTS

Verification of three-dimensional image registration using bony anatomy projection patterns

The result from the phantom studies showed that the residual errors were -0.06 ± 0.34 mm in the RL direction, -0.10 ± 0.42 mm in the AP direction, and 0.42 ± 0.45 mm in the CC direction. The voxel size was $1.02 \times 1.02 \times 1.25$ mm^3, showing that the accuracy of our registration method was within the voxel size.

Gross tumor volume

Figure 2 illustrates the interfraction variations in the GTV volume at EE among the sessions. The σ of the GTV was 0.59 cm^3 at EI and 0.53 cm^3 at EE, smaller than the GM of 6.62 cm^3 at EI and 6.70 cm^3 EE or the Σ of 3.04 cm^3 at EI and 3.21 cm^3 at EE. The GTV variations among the sessions were not significant at either EI (p = .301) or EE (p = .081).

GTV motion range

Figure 3 shows the interfraction variations in the GTV motion range among the three sessions. The random variations in the GTV motion range for the upper lobe in the RL and AP directions were within 1 mm and that for the lower lobe in the CC direction was 3.40 mm. No significant differences in the GTV motion range were seen among the three sessions (p = .930, RL; p = .983, AP; and p = .293, CC). The motion range along the CC direction was significantly larger than that along the RL direction ($p < .01$) or the AP direction ($p < .01$). The motion range (11.72 ± 4.47 mm) for the lower lobe was significantly larger than the motion range (1.44 ± 1.39 mm) for upper lobe in the CC direction.

GTV centroid position

Figure 4 presents the interfraction variations in the GTV centroid positions at EE among the sessions in each direction. Greater variations in the GTV centroid position at EE in the

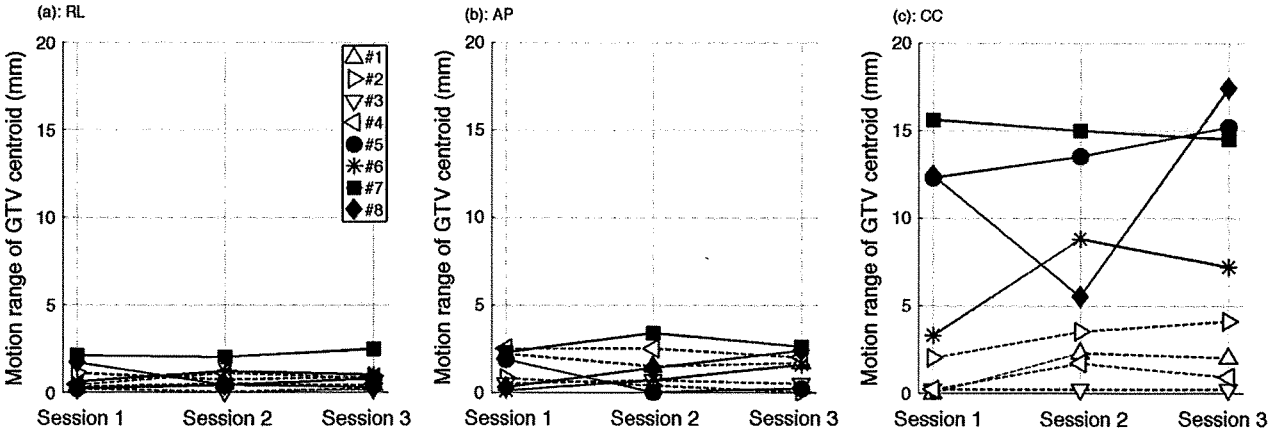

Fig. 3. Interfraction variations in gross tumor volume motion range defined as distance from gross tumor volume centroid position at end-inhalation to that at end-exhalation among three sessions in (a) right–left (RL), (b) anteroposterior (AP), and (c) craniocaudal (CC) directions. Dashed lines indicate variations for upper lobe tumors; solid lines, variations for lower lobe tumors. In any direction, significant differences in gross tumor volume motion range were not seen among sessions (p = .930, RL; p = .983, AP; and p = .923, CC).

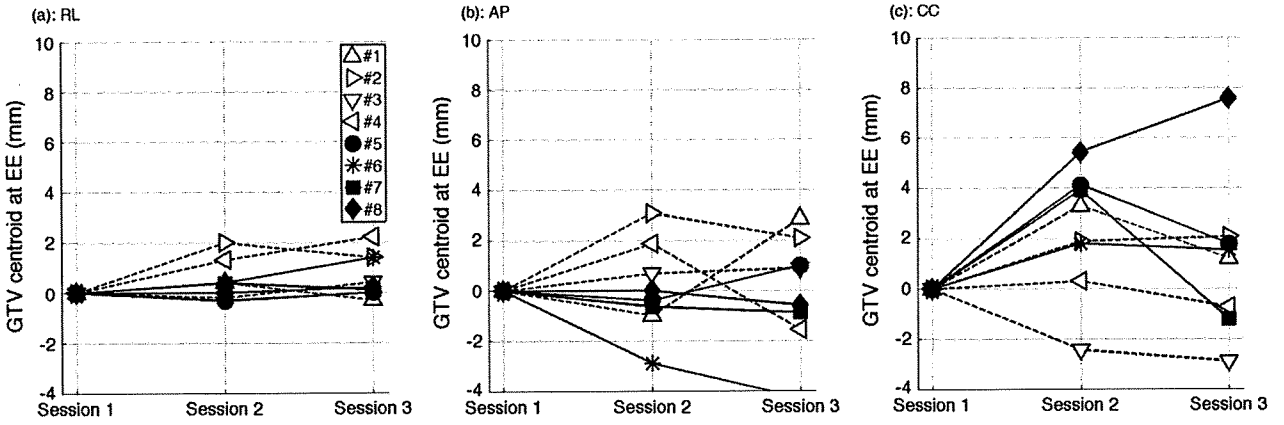

Fig. 4. Interfraction variations in gross tumor volume centroid positions at end-exhalation among sessions in (a) right–left (RL), (b) anteroposterior (AP), and (c) craniocaudal (CC) directions. Dashed lines indicate variations for upper lobe tumors; solid lines, variations for lower lobe tumors. Greater tumor motions seen in AP and CC directions than in RL direction; however, they were almost within 5 mm and no significant displacement in gross tumor volume were observed among sessions.

AP and CC directions were seen than those in the RL direction; however, no significant displacement of the GTV centroid position was observed among the sessions in the RL (p = .068), AP (p = .979), or CC (p = .078) direction. Also, no significant displacements of the GTV centroid position at EI were seen among the sessions in the RL (p = .712), AP (p = .970), or CC (p = .128) direction.

Table 2 lists the mean and SD of the GTV centroid displacement among the sessions at EE and EI. The variation of GTV centroid displacement at EE for the lower lobe in the CC direction was larger than that in other directions, and significant differences in the GTV centroid displacement between the lower and upper lobes were not observed in the RL (p = .058), AP (p = .503), and CC (p = .097) directions. The SD of the GTV centroid displacement at EI for the lower lobe in the CC direction was much larger than that at EE, and the SD of the GTV centroid displacements in the RL and AP directions was not different between EI and EE.

The GM, Σ, and σ at both EE and EI are listed in Table 3. The Σ and σ at EI were slightly larger than at EE in the CC direction and were almost same in the other directions.

iGTV and centroid position

The σ (0.83 cm^3) of the iGTV volume was smaller than the GM (11.11 cm3) or the Σ (4.58 cm^3). Moreover, the σ of the iGTV centroid position in the RL (0.61 mm), AP (1.27 mm), and CC (1.86 mm) directions were the same or smaller than the Σ in the RL (0.61 mm), AP (1.70 mm), and CC (2.44 mm) directions, respectively.

DISCUSSION

Bony anatomy registration verification

From the phantom study, the registration technique using the bony anatomy projection patterns had an accuracy of 1 voxel size, leading to correct setup error. The residual errors in the CC direction were larger than in the RL and AP directions. This might have resulted from the partial volume effect included by differences in the voxel size. The registration technique is susceptible to the threshold for bony anatomy binarization; therefore, careful attention should be paid to selecting the bony anatomy threshold level. In the present study, we chose the threshold level to extract bony region correctly by visual evaluation.

The accuracy of this algorithm also tended to be reduced in the presence of patient movement, such as respiration and transformation of the bony structures. The patients in the present study were immobilized firmly with the SBF and large transformations in bony structure were not seen; thus, we estimated the setup errors only for the rigid body.

Reliability of 4D-CT

Motion artifacts might have degraded the results of the present study. We used 4D-CT with an image-binning

Table 2. GTV centroid displacement among the sessions at end-exhalation and at end-inhalation

	RL (mm)		AP (mm)		CC (mm)	
	Upper	Lower	Upper	Lower	Upper	Lower
EE	1.03 ± 0.81	0.36 ± 0.45	1.75 ± 0.90	1.34 ± 1.47	1.85 ± 1.05	3.42 ± 2.25
EI	0.85 ± 0.60	0.69 ± 0.42	1.39 ± 0.98	2.04 ± 1.80	1.27 ± 1.26	3.70 ± 3.75

Abbreviations: GTV = gross tumor volume; RL = right–left; AP = anteroposterior; CC = craniocaudal; EE = end-exhalation; EI = end-inhalation.

Data presented as mean ± standard deviation.

Table 3. Group mean, systematic variation, and random variation in GTV displacement at end-exhalation and end-inhalation

	RL (mm)		AP (mm)		CC (mm)	
	EE	EI	EE	EI	EE	EI
GM	0.59	0.19	0.02	−0.11	1.73	0.71
Σ	0.77	0.86	1.77	2.12	2.61	3.31
σ	0.45	0.55	1.41	1.38	1.62	2.98

Abbreviations: GM = group mean; Σ = systematic variation; σ = random variation; other abbreviations as in Table 2.

technique, in which the CT images were acquired in cine mode using a CT scanner (15). This type of technique in 4D-CT imaging can lead to motion artifacts, because the data acquisition at each couch position is initially independent of the actual respiratory state owing to the irregular breathing of the patient. To address these problems, we used images at EI and EE in which the interfraction variations in the GTV were considered small.

Interfraction variations in GTV and iGTV

Despite a high dose per session for hypofractionated SBRT, the interfraction variations in the GTV revealed that the volume, motion range, and centroid position at EI and EE did not vary significantly. For the iGTV, a similar result was obtained. A little change in the GTV during the 2- or 3-week period was similar to that in previous reports, in which significant changes in the target volume occurred after ≥2 weeks (8, 9, 16, 17). A time trend in the tumor motion range was not observed during the treatment course, just as other research has reported (8, 9, 11, 12, 18–20).

The systematic and random variations in GTV displacement in our results were slightly smaller than those reported by Sonke *et al.* (11). We used the SBF to reduce the intrafraction patient motion and improve the reproducibility of the interfraction patient position. In contrast, Sonke *et al.* (11) did not used any immobilization device. Use of the SBF might have decreased the systematic and random variations in GTV displacement.

The GTV motion range in the lower lobe along the CC direction was significantly larger than in the upper lobe, as reported by Seppenwoolde *et al.* (7), Onimaru *et al.* (21), and Liu *et al.* (22). The interfraction variations in the GTV centroid position in the CC direction were slightly larger than in the RL and AP directions at EI and EE. Moreover, the SD of the GTV displacement in the lower lobe at EI was larger than at EE, suggesting that the GTV position at EI might vary much more than at EE in the lower lobe.

Tumors at the bottom end of the lower lobe showed a large interfraction variation in the GTV position along the CC direction in the present study. This might have resulted from the tumor location. Tumor close to the diaphragm moves with a wide range, according to the motion of the diaphragm (7). Moreover, a high tumor motion velocity can increase the motion artifacts on 4D-CT images, leading to inaccurate delineation of the GTV. We believe these factors invoked large interfraction variations in the GTV position. During treatment, the dose delivery to the patient was performed while the patient's upper abdomen remained pressed by a diaphragm control. Also, the setup errors and tumor position changes in the patient were corrected by comparing the portal images and digitally reconstructed radiographs. These processes reduced target mispositioning. In such cases, a repeated 4D-CT scan during the treatment course is useful to confirm that the PTV contains all the target volumes. Because the PTV margin is added systematically for all patients, it might be too large for some patients or too small for others. An additional approach is needed to assess the margin size. Also, our conclusions must be verified because of the small patient numbers.

CONCLUSION

We investigated the interfraction variations in volume, motion range, and position of GTV during hypofractionated SBRT for lung cancer using 4D-CT with a SBF. Large interfraction variations in the GTV, motion range, and position were observed only seldom; however, the position of the GTV centroid in the CC direction had a marginally larger variation than that in any other directions for tumor at the bottom end of the lower lobe.

REFERENCES

1. Nagata Y, Negoro Y, Aoki T, *et al.* Clinical outcomes of 3D conformal hypofractionated single high-dose radiotherapy for one or two lung tumors using a stereotactic body frame. *Int J Radiat Oncol Biol Phys* 2002;52:1041–1046.
2. Onishi H, Araki T, Shirato H, *et al.* Stereotactic hypofractionated high-dose irradiation for stage I nonsmall cell lung carcinoma: Clinical outcomes in 245 subjects in a Japanese multiinstitutional study. *Cancer* 2004;101:1623–1631.
3. Takayama K, Nagata Y, Negoro Y, *et al.* Treatment planning of stereotactic radiotherapy for solitary lung tumor. *Int J Radiat Oncol Biol Phys* 2005;61:1565–1571.
4. Nagata Y, Matsuo Y, Takayama K, *et al.* Current status of stereotactic body radiotherapy for lung cancer. *Int J Clin Oncol* 2007;12:3–7.
5. International Commission on Radiation Units and Measurements. ICRT report 62, Prescribing, recording and reporting photon bream therapy (supplement to ICRU report 50). Bethesda: ICRU; 1999.
6. Mageras GS, Pevsner A, Yorke ED, *et al.* Measurement of lung tumor motion using respiration-correlated CT. *Int J Radiat Oncol Biol Phys* 2004;60:933–941.
7. Seppenwoolde Y, Shirato H, Kitamura K, *et al.* Precise and real-time measurement of 3D tumor motion in lung due to breathing and heartbeat, measured during radiotherapy. *Int J Radiat Oncol Biol Phys* 2002;53:822–834.
8. Bosmans G, Baardwijk A, Dekker A, *et al.* Intra-patient variability of tumor volume and tumor motion during conventionally fractionated radiotherapy for locally advanced non–small-

cell lung cancer: A prospective clinical study. *Int J Radiat Oncol Biol Phys* 2006;66:748–753.
9. Britton KR, Starkschall G, Tucker SL, *et al.* Assessment of gross tumor volume regression and motion changes during radiotherapy for non–small-cell lung cancer as measured by four-dimensional computed tomography. *Int J Radiat Oncol Biol Phys* 2007;68:1036–1046.
10. Juhler-Nøttrup T, Korreman SS, Pedersen AN, *et al.* Interfractional changes in tumour volume and position during entire radiotherapy courses for lung cancer with respiratory gating and image guidance. *Acta Oncol* 2008;47: 1406–1413.
11. Sonke JJ, Lebesque J, van Herk M. Variability of four-dimensional computed tomography patient models. *Int J Radiat Oncol Biol Phys* 2008;70:590–598.
12. Michalski D, Sontag M, Li F, *et al.* Four-dimensional computed tomography-based interfractional reproducibility study of lung tumor intrafractional motion. *Int J Radiat Oncol Biol Phys* 2008;71:714–724.
13. Nakamura M, Narita Y, Matsuo Y, *et al.* Geometrical differences in target volumes between slow CT and 4D CT imaging in stereotactic body radiotherapy for lung tumors in the upper and middle lobe. *Med Phys* 2008;35: 4142–4148.
14. Negoro Y, Nagata Y, Aoki T, *et al.* The effectiveness of an immobilization device in conformal radiotherapy for lung tumor: Reduction of respiratory tumor movement and evaluation of the daily setup accuracy. *Int J Radiat Oncol Biol Phys* 2001; 50:889–898.
15. Rietzel E, Pan T, Chen GT. Four-dimensional computed tomography: Image formation and clinical protocol. *Med Phys* 2005; 32:874–889.
16. Underberg RW, Lagerwaard FJ, van Tinteren H, *et al.* Time trends in target volumes for stage I non–small-cell lung cancer after stereotactic radiotherapy. *Int J Radiat Oncol Biol Phys* 2006;64:1221–1228.
17. Woodford C, Yartsev S, Dar AR, *et al.* Adaptive radiotherapy planning on decreasing gross tumor volumes as seen on megavoltage computed tomography images. *Int J Radiat Oncol Biol Phys* 2007;69:1316–1322.
18. Chang J, Mageras GS, Yorke E, *et al.* Observation of interfractional variations in lung tumor position using respiratory gated and ungated megavoltage cone-beam computed tomography. *Int J Radiat Oncol Biol Phys* 2007;67:1548–1558.
19. Jensen HR, Hansen O, Hjelm-Hansen M, *et al.* Inter- and intrafractional movement of the tumour in extracranial stereotactic radiotherapy of NSCLC. *Acta Oncol* 2008;47:1432–1437.
20. Hugo GD, Liang J, Campbell J, *et al.* On-line target position localization in the presence of respiration: A comparison of two methods. *Int J Radiat Oncol Biol Phys* 2007;69:1634–1641.
21. Onimaru R, Shirato H, Fujino M, *et al.* The effect of tumor location and respiratory function on tumor movement estimated by real-time tracking radiotherapy (RTRT) system. *Int J Radiat Oncol Biol Phys* 2005;63:164–169.
22. Liu HH, Balter P, Tutt T, *et al.* Assessing respiration-induced tumor motion and internal target volume using four-dimensional computed tomography for radiotherapy of lung cancer. *Int J Radiat Oncol Biol Phys* 2007;68:531–540.

New algorithm to simulate organ movement and deformation for four-dimensional dose calculation based on a three-dimensional CT and fluoroscopy of the thorax

Yuki Miyabe,[a] Yuichiro Narita, Takashi Mizowaki, Yukinori Matsuo, and Kenji Takayama
Department of Radiation Oncology and Image-Applied Therapy, Kyoto University Graduate School of Medicine, Kyoto 606-8507, Japan

Kunio Takahashi, Shuji Kaneko, and Noriyuki Kawada
Medical Systems Administration Office, Hiroshima Machinery Works, Mitsubishi Heavy Industries, Limited, Hiroshima 733-8553, Japan

Akira Maruhashi
Department of Radiation Life Science and Radiation Medical Science, Research Reactor Institute, Kyoto University, Osaka 590-0494, Japan

Masahiro Hiraoka
Department of Radiation Oncology and Image-Applied Therapy, Kyoto University Graduate School of Medicine, Kyoto 606-8507, Japan

(Received 22 December 2008; revised 16 June 2009; accepted for publication 20 July 2009; published 4 September 2009)

Purpose: The aim of this study was to develop a 4D-modeling algorithm, designated "3D+," to simulate organ movement and deformation for 4D dose calculation without the need for 4D-CT or deformable image registration and to assess the validity of this algorithm.
Methods: This 3D+ algorithm virtually creates 4D-CT images by deforming static 3D-CT data according to a typical motion model and motion data at multiple observation points collected via fluoroscopy. A typical motion model intended for patients with lung tumors immobilized with a vacuum pillow inside a stereotactic body frame was constructed. The geometric accuracy of virtual 4D-CT images created using this 3D+ algorithm was evaluated in eight patients by comparing the simulated results with actual 4D-CT images in terms of visual assessment, landmark analysis, and comparison of the radial distance from the tumor centroid to the body or lung surface.
Results: The average accuracy for all patients, as determined via landmark analysis, was 2.8 ± 1.8 mm, very similar to results obtained through 4D-CT and deformable image registrations. Error in the radial distance from the tumor centroid to the body or lung surface was generally within 1.0 or 2.0 mm, respectively, in virtual versus actual 4D-CT images. Therefore, it is assumed that these geometric errors would have only negligible effects on dose calculation.
Conclusions: 4D modeling of the thorax utilizing the 3D+ algorithm shows acceptable accuracy and is more suited for routine clinical use in terms of processing time than conventional 4D-CT and deformable image registration. The 3D+ algorithm may be useful for simulating dose distribution for advanced beam delivery techniques, such as real-time tumor tracking irradiation and adaptive radiation therapy. © *2009 American Association of Physicists in Medicine.*
[DOI: 10.1118/1.3213083]

Key words: organ motion, deformable modeling, 4D-CT, lung tumor

I. INTRODUCTION

Respiratory motion in the thorax and upper abdomen can be a significant source of error in radiation delivery during external-beam radiotherapy.[1–3] Respiratory motion can also cause artifacts, such as distortions in the target and organ at risk (OAR) volumes in a conventional three-dimensional (3D) computed tomography (CT) image set.[4] Traditional methods to address tumor motion in radiotherapy involve setting an adequate margin around the clinical target volume (CTV) when defining the planning target volume (PTV).[5] Organ motion is assessed via fluoroscopy or serial CT scans taken at different phases of respiratory movement either during the simulation or beforehand.

In the current standard procedure for radiotherapy treatment planning, doses are prescribed to the PTV using a static patient model (simulation CT scans). As a result, some discrepancies between the planned and actual delivered dose distributions may occur,[6] which may result in the misinterpretation of dose-volume data in relation to clinical outcomes. Therefore, to properly account for the time-dependent variations in geometry, dose calculations should be performed using multiple models representing each phase of the respiratory cycle in the same patient. In addition, for clinical applications using advanced beam delivery techniques, such as real-time tumor tracking irradiation, it is imperative to simulate dose distribution in multiple-phase mod-

els. In this case, four-dimensional (4D)-CT is appropriate because it provides multiple-phase models directly.[7–10] However, although 4D-CT contains a complete description of the patient geometry for each respiratory phase, this technique does not describe how the tissues move and deform from phase to phase. Therefore, the 4D-CT images are insufficient alone and require an additional deformable image registration tool.[11–13] Deformable image registration is a technique that accounts for internal organ deformation and plays a crucial role in mapping and combining doses received by the same volume in each phase of the respiratory cycle. Combining 4D-CT and deformable image registrations allows more accurate calculation of dose distributions in the tumor and critical organs because it is possible to sum the doses delivered to a volume during different phases of the respiratory cycle while accounting for the effects of organ motion and deformation.[14–16] However, 4D-CT scans are not widely available, and the currently available commercial treatment planning systems cannot perform deformable image registration. Deformable image registration remains a difficult and time-consuming task and is generally impractical for routine clinical use.[17–20]

Therefore, we devised an alternate method of generating a 4D model (i.e., multiple-phase image sets that are geometrically related to one another) without using 4D-CT or deformable image registration. In this method, a patient model at any phase during free breathing was produced by deforming a static 3D-CT. Deformation was performed based on a typical motion model built from accumulated knowledge of anatomy, and the amplitude of movement was determined by estimates from fluoroscopic data sets. This novel method, designated "3D+," generates a 4D model by adding movement data to a 3D-CT data set.

The 3D+ algorithm requires static 3D-CT data and a temporal fluoroscopic image set. In addition, specific knowledge regarding the mechanics of breathing is preferred to construct a typical motion model.[21,22] Because the respiratory motion of the internal organs varies according to body position (supine or prone), the position of the arms, and the type of immobilization devices,[23] the program used for 4D modeling also varies according to these conditions. In this article, we provide a detailed description of a thoracic 3D+ model aimed at lung cancer treatment, and we verified the accuracy of this model by comparing it to actual 4D-CT data.

II. MATERIALS AND METHODS

A 3D+ algorithm for thoracic 4D modeling was developed based on a static 3D-CT data set and temporal fluoroscopic imaging.

II.A. Concept of the 3D+ algorithm

The 3D+ is an algorithm that creates a 3D-CT image set for an arbitrary breathing phase through deformation of a static 3D-CT image according to patient-specific motion patterns and amplitudes. Motion data are assessed and collected via orthogonal fluoroscopic imaging. However, fluoroscopic imaging is insufficient to generate a 4D model because these data are limited to two-dimensional (2D) projections, whereas respiratory motion is 3D. Therefore, fluoroscopic motion data were complemented with a typical motion model built from anatomical knowledge. Then, a transformation map illustrating the vectors involved in shifting and distorting the 3D-CT image from one specific phase to another was computed by inputting the amplitude of movement at specific observation points intended to characterize kinetic changes into a typical motion model.

A flowchart of the process required to generate a 4D model using the 3D+ algorithm is shown in Fig. 1. The motion data for a single breathing cycle and trajectories are obtained as an average pattern from continuous breathing curves at each observation point (e.g., tumor centroid and top position of the diaphragmatic dome). These data are used to represent displacement due to respiratory motion in the 3D + algorithm. An original 3D-CT set is required only at a specific breathing phase and is acquired using respiratory-triggered or breath-holding methods to reduce artifacts due to respiratory motion. The digitally reconstructed radiograph (DRR) of the original 3D-CT is compared to sequential fluoroscopic images to identify the breathing phase that corresponds to a given CT phase. Then the number of phase divisions (n) and their positions are determined to generate 4D-CT data sets. The transformation map, which illustrates the shift from the reference phase to each selected phase, is calculated based on displacement vectors for certain "lattice-shaped" points; the displacement of these points is calculated from the estimated average motion data of observation points and the typical motion model. Each point $\mathbf{r}=(x,y,z)$ moves according to its own vector for phase i $[\mathbf{T}_i(\mathbf{r})]$, and the CT value (Hounsfield number) at each point is modified based on density fluctuation as follows:

$$\mathbf{r}' = \mathbf{r} + \mathbf{T}_i(\mathbf{r}),$$

$$I_i(\mathbf{r}') = (I_{\text{org}}(\mathbf{r}) + 1000) \times D_i(\mathbf{r}') - 1000, \quad (1)$$

where $\mathbf{T}_i$ is the transformation vector from the original 3D-CT image to the simulated CT image for each of the selected phase i $\{i=1,\ldots,n\}$, and $\mathbf{r}$ and $\mathbf{r}'$ are the position vectors of points in the original and created CT images, respectively. The x, y, and z directions correspond to the right-left (RL), anterior-posterior (AP), and superior-inferior (SI) directions, respectively. Both I_{org} and I_i are the pixel values (CT number) at each point. D_i is the grid density relative to the density of the original lattice-shaped points, which represents the change in density associated with deformation. Because elastic structures are limited to soft tissue in most cases, the relationship between CT number and density in Eq. (1) is assumed to conform to the following equation:[24]

$$\rho_e = 1.0 + 0.001 \times \text{CT number}, \quad (2)$$

where ρ_e is the electron density relative to the electron density of water. The 3D-CT sets of each selected phase are created by reconstructing the alignment of pixels, and then pixel values are calculated using nearest-neighbor interpolation or bilinear interpolation.

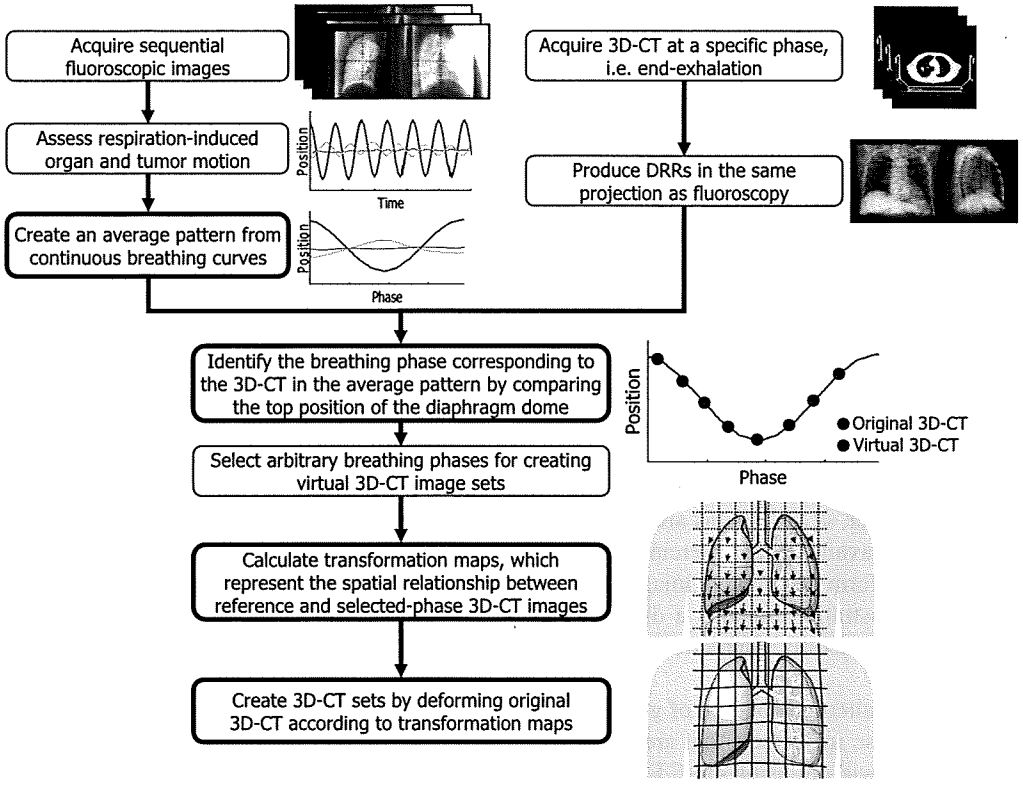

FIG. 1. Flowchart showing the process required to generate a 4D model using the 3D+ algorithm. The boxes outlined in boldface represent automated processes.

II.B. 4D modeling of the thorax in the supine position

We constructed a typical motion model intended to represent patients with lung tumors immobilized with a vacuum pillow inside a stereotactic body frame (SBF; Elekta Corp., Stockholm, Sweden) in the supine position with their arms elevated. In principle, the 3D+ algorithm was developed to account for respiratory motion, so transformations due to heartbeat, deglutition, and body motion were ignored.

II.B.1. Biomechanical motion of breathing

The thoracic respiratory muscles consist of the intercostals and diaphragm, which are mainly related to costal and abdominal respiratory movements, respectively. Because the lungs and surrounding chest wall move independently of each other at the pleural interface, patient volume is segmented into two independent movable components: Organs inside the thoracic cage (i.e., lungs, heart, mediastinum, diaphragm, and liver) and the thoracic wall (thoracic vertebrae, ribs, sternum, skin, muscle, etc.). The former component moves according to contraction or relaxation of the diaphragm and intercostal muscles, whereas the latter moves only according to the intercostal muscles. In the lung field, large movement and deformation are observed in the lower lobe, whereas the upper lobe is relatively stable. In addition, the dorsal diaphragm generally moves more widely than the ventral diaphragm when in the supine position. Outside the thoracic cage, the thoracic vertebrae are almost completely immobilized. The contraction of intercostal muscles generates rib movement and, through mechanical linkage, generates movement in the diaphragm and abdominal wall. The front ends of the ribs move either upward and forward or downward and backward along with the sternum, and each rib shows either outward or inward rotation around an imaginary line joining its two ends. These movements result in vertical and transverse widenings or narrowings of the thoracic cage.

II.B.2. Typical motion model

Based on the biomechanical motion of breathing, a typical motion model of the thorax is configured, and relevant observation points on fluoroscopic images are determined. Observation points are selected from the easily discernible sites on fluoroscopic images. In addition, the positions of observation points should be specified on the 3D-CT. Fluoroscopic measurements should be performed in more than two directions to generate 3D motion data. In this instance, orthogonal frontal and lateral fluoroscopic images are used; the observation points in the thorax of a representative lung cancer patient are displayed in Fig. 2. To promote speed and efficiency, the minimum number of observation points is used. That is, all the discernible points on fluoroscopic images were initially extracted, for example, lung boundaries, ribs, and bronchi. Thereafter, we removed redundant points such as those whose position could be obtained from that of other observation points. For example, the rib position can be obtained from that of the chest wall, and the bronchus position